SELECTIVE HYDROGENATION OF LIGNIN-DERIVED MODEL COMPOUNDS TO PRODUCE NYLON 6 PRECURSORS

A Thesis
Presented to
The Academic Faculty

by

Xiaojuan Zhou

In Partial Fulfillment
of the Requirements for the Degree
Master of Science in Chemical Engineering in the
School of Chemical & Biomolecular Engineering

Georgia Institute of Technology
December 2013

SELECTIVE HYDROGENATION OF LIGNIN-DERIVED MODEL COMPOUNDS TO PRODUCE NYLON 6 PRECURSORS

Approved by:

Dr. Christopher Jones, Advisor
School of Chemical & Biomolecular Enginering
Georgia Institute of Technology

Dr. Carson Meredith
School of Chemical & Biomolecular Engineering
Georgia Institute of Technology

Dr. Pradeep Agrawal, Advisor
School of Chemical & Biomolecular Engineering
Georgia Institute of Technology

Dr. Charles Liotta
School of Chemistry and Biochemistry
Georgia Institute of Technology

Date Approved: August 14, 2013

To my parents Li and Weibin,
who made it all possible

ACKNOWLEDGEMENTS

Foremost, I would like to express my sincere gratitude to my advisors Prof. Pradeep K. Agrawal and Prof. Christopher W. Jones for the continuous support of my study and research, for their patience, encouragement, enthusiasm, and invaluable expertise they shared with me. Their guidance helped me in all the time of research and writing of this thesis. Next, I would like to thank my committee members, Prof. Carson Meredith and Prof. Charles Liotta, for their time of reading my thesis and providing insightful comments. I would also like to thank all the members of the Jones group. The generous help they gave me throughout two years taught me the values of teamwork and friendship. Special thanks go to the following individuals: Weiyin for sharing her knowledge and for her company in Bunger-Henry; Mike for helping with instrument problems when they arose, as well as running XAS of my samples; Nick and Miles for helping me build a Parr reactor; and Megan for running the TEM of my samples. Last but certainly not the least, I would like to thank my parents, who have always been my moral support, who share joy with me and stand by me through hard times. To all of you who helped me make it possible: I give you my deepest gratitude.

TABLE OF CONTENTS

LIST OF TABLES

LIST OF FIGURES

CHAPTER 1

INTRODUCTION

1.1 Motivation

According to 1996 Noble Prize winner Richard E. Smalley, energy is the most pressing problem on the list of "Top Ten Problems of Humanity in the Next 50 Years" [1]. The main energy concerns are the depletion of petroleum as well as climate change caused by CO_2 emissions from petroleum coal and natural gas usage. Petroleum, according to a survey from the IEA in 2012, still produced almost one third of the world's energy [2]. Figure 1.1.1 shows that in 2010, 81.1% of the world energy consumption was from non-renewable sources including oil (32.4%), coal and peat (27.3%) and gas (21.4%). The amount of oil consumed increased from 2,819 million tons to 4,120 million tons from 1973 to 2010 [2]. The average increase was about 1.2% per year.

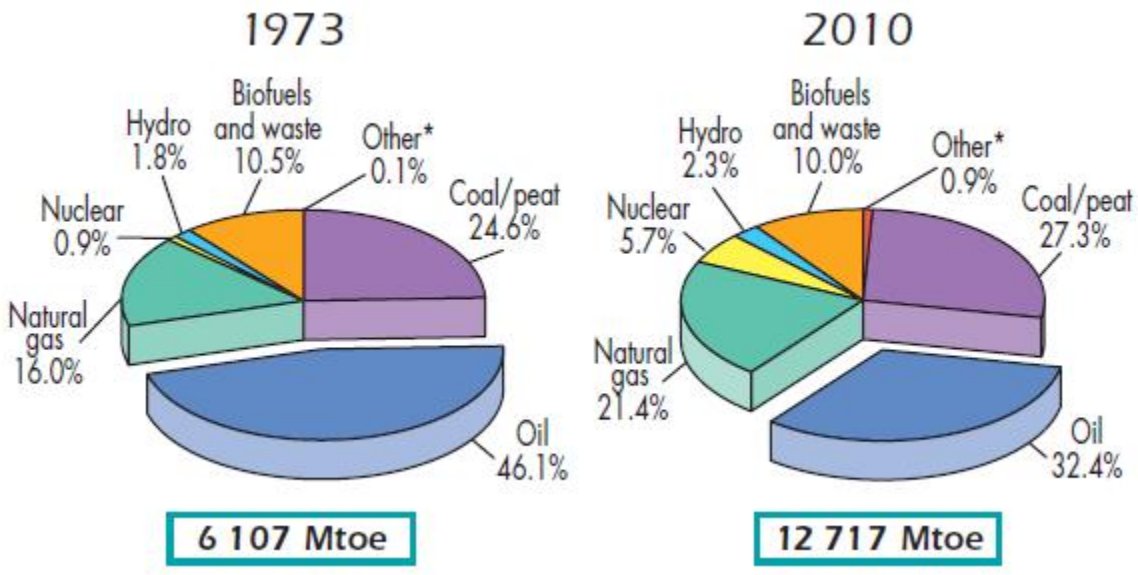

Figure 1.1.1 Total world consumption of primary energy in 1973 and 2010 [2]

However, the world supply of petroleum is depleting. Figure 1.1.2 shows the world oil discoveries and consumption from 1900 to 2007 [3]. The volume of oil discovery peaked around 1957. Up to 2007, 61 vol% of previously discovered oil had been consumed. According to the authors' model, world oil demand would increase at an average rate of 1.2% per year, and eventually the demand will overtake the capacity of the producing fields and the volume of oil that could potentially be discovered [3].

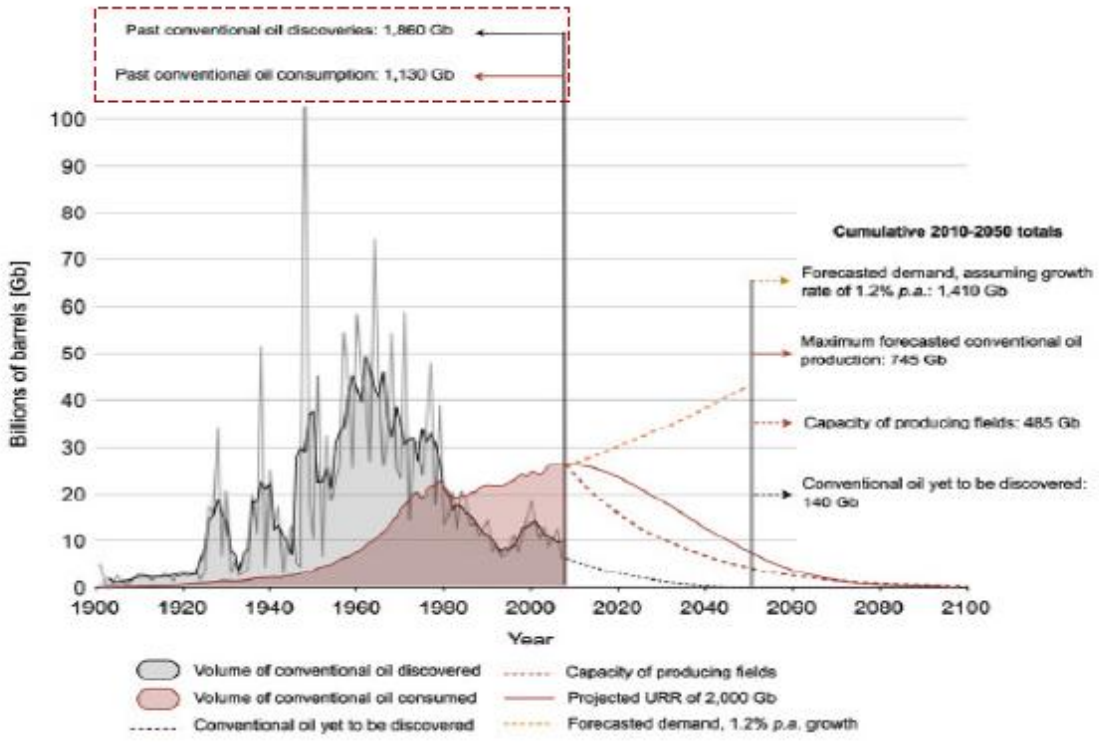

Figure 1.1.2 Annual proven and probable reserves (2P), backdated oil consumption, discoveries, forecasted consumption and forecasted production till 2100 [3]

It is thus important that alternative sources to crude oil for liquid fuels be developed. Suitable alternative resources should be renewable, readily available and sustainable. Solar, nuclear, geothermal, wind, and biomass are some resources currently under development as alternate energy sources [2]. Among these, biomass, including sugar,

vegetable oil, and animal fat, can be converted to liquid fuels, which can to be processed within the current petroleum infrastructure [4].

According to Key World Energy Statistics 2012, the United States was the world's largest net importer of crude oil [2]. This makes the country easily impacted by changes in the foreign oil trade, which is not good for the country's energy security [5]. In the 1950s M. Hubbert predicted that the US oil supply would start diminishing in the next 50 years [6, 7] and proposed a model that reflects the overall actual crude oil production in the US [8]. It can be seen in Figure 1.1.3 that the highest oil production was in 1972 and has been decreasing since the late 1970s up to 2009. The increase since 2009 might be due to expansion in oil exploration and drilling, as well as the application of hydraulic fracturing techniques [9].

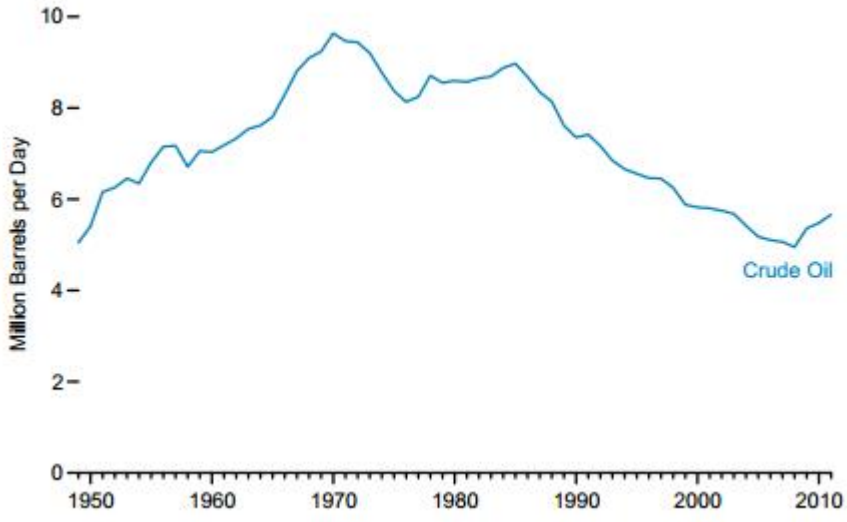

Figure 1.1.3 Crude oil well productivity in the US, 1949-2011 [8]

Due to the reduction in crude oil production, the US General Accountabilities Office published a report in 2007 focusing not only on enhancing current oil recovery but also

sourcing production from alternative non-conventional fuels such as corn ethanol, biomass, coal and hydrogen [10]. In 2010, the US Environmental Protection Agency finalized the regulations relating to the National Renewable Fuel Standard Program and set volume standards for specific types of renewable biofuels including cellulosic, biomass-based diesel and total advanced biofuels [5].

Biomass is a renewable, readily available resource. It was the main energy resource in the world before the advent of fossil fuels. One of wood's major usages was for energy generation through combustion [11]. Oak Ridge National Laboratory reported in 2005 that there were about a billion tons of biomass, from both forest and agricultural lands, for possible use in biofuel production in the US [12]. Biomass is typically processed through biochemical and thermochemical routes to yield liquid biofuels for transportation use.

Currently biomass-derived fuels are divided into first-generation, second-generation and third-generation biofuels [4]. First-generation biomass includes liquid biofuels from starch, sugar and fatty acid oils [13]. Ethanol from corn is one of the most well-known first-generation biofuels. First-generation biofuel technologies have been developed to relative maturity; however, their competition with food use causes price increases and the heavy usage of water in the fuel generating processes make first-generation biofuels unsustainable [13]. Second-generation biofuels are made from biomass feedstock such as lignocellulosic plants, agricultural and forest residues and other non-food energy crops [14, 15]. In World Energy Outlook 2010, the International Energy Agency forecasted that second-generation and advanced biofuels would enter the market in 2010 [16]. However, there is still doubt about whether second-generation biofuels can provide enough

transportation fuel to justify biomass transportation to large production facilities. Meanwhile the technologies for utilizing second-generation biomass are still immature and there is space for cost reduction and production efficiency improvement [15, 17]. Third-generation biofuels can be sourced from algae and animal fat through biological or chemical catalytic processes [4]. Third-generation biofuels have the potential of providing three to five times more recoverable energy than first and second-generation biofuels without damaging the environment or economy [14, 18].

The world consumption of petroleum by sectors is shown in Figure 1.1.4 [2]. It can be seen that aside from petroleum's familiar use as an energy source, it also has importance in non-energy use, which increased from 11.6% of total consumption to 17.1% from 1973 to 2010. Non-energy use was defined as "those fuels that are now used as raw materials in the different sectors and are not consumed as a fuel or transformed into another fuel" [2]. One of the most important non-energy uses of petroleum is as a chemical feedstock for polymers and production of other chemicals. As fossil fuel reserves diminish and world energy demand increases, it is crucial to search for alternative sources to supplement petroleum as both a fuel and chemical feedstock. The most obvious option is biomass. High value products such as lactic acid, bioethanol, levulinic acid, lipids and vanillin can be obtained from lignocellulosic biomass conversion through catalytic upgrading [14, 19, 20].

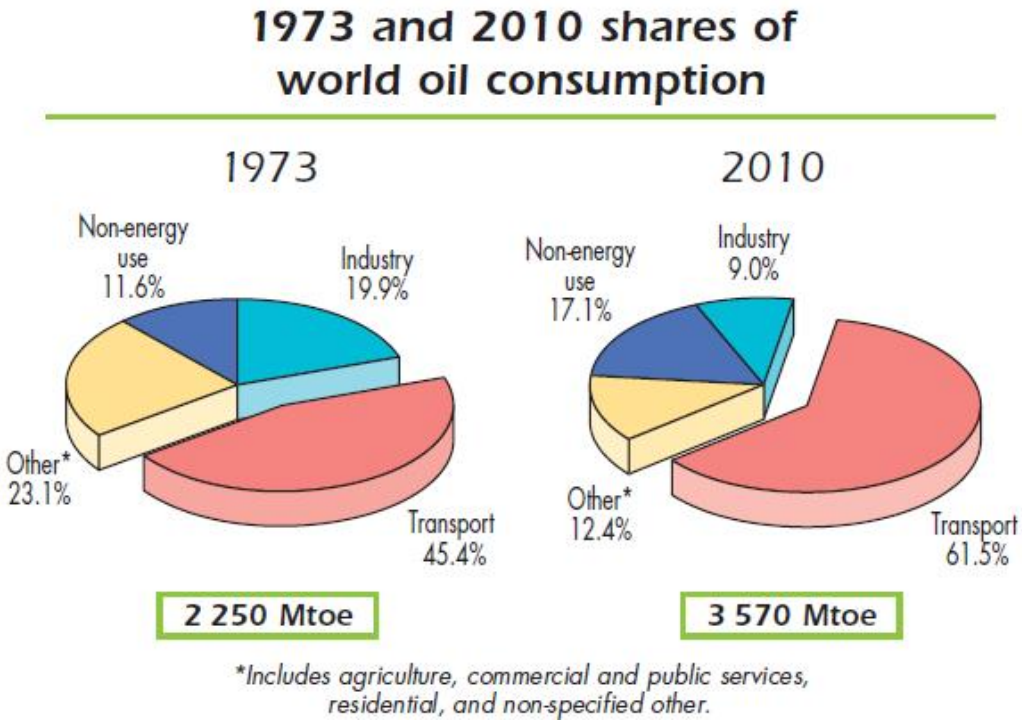

Figure 1.1.4 World total final oil consumption by sector, 1973 and 2010 [2]

A list of chemicals that can be sourced from sugar and lignin was published in 2004 by the Pacific Northwest National Laboratory and National Renewable Energy Laboratory [21].

1.2 Lignin

Lignocellulosics are second-generation biomass feedstock and are composed of three major types of polymers: cellulose, hemicellulose and lignin [22, 23]. In lignocellulosic biomass, cellulose and hemicellulose are primarily used for papermaking, as well as industrial polymers and bio-ethanol. Lignin, which comprises one third of lignocellulosic biomass, is left behind as a by-product. Paper industries pay to have lignin removed from sites for burning to provide heat and power. However, it has a high potential to produce

not only heat and power but also carbon fibers, aromatic hydrocarbons (benzene, toluene, xylene), and fine chemicals, such as vanillin, phenol, phenol resins, etc. [24].

The chemical structure of lignin is very different from the carbohydrates: it is amorphous and poly-aromatic. Till now there is no consensus on the actual lignin structure, due to the changes of lignin structure in different plants such as softwood, hardwood, grass, etc. as well as the chemical content change caused by different methods used to extract lignin from wood. Figure 1.2.1 shows a representative softwood lignin structure [25, 26].

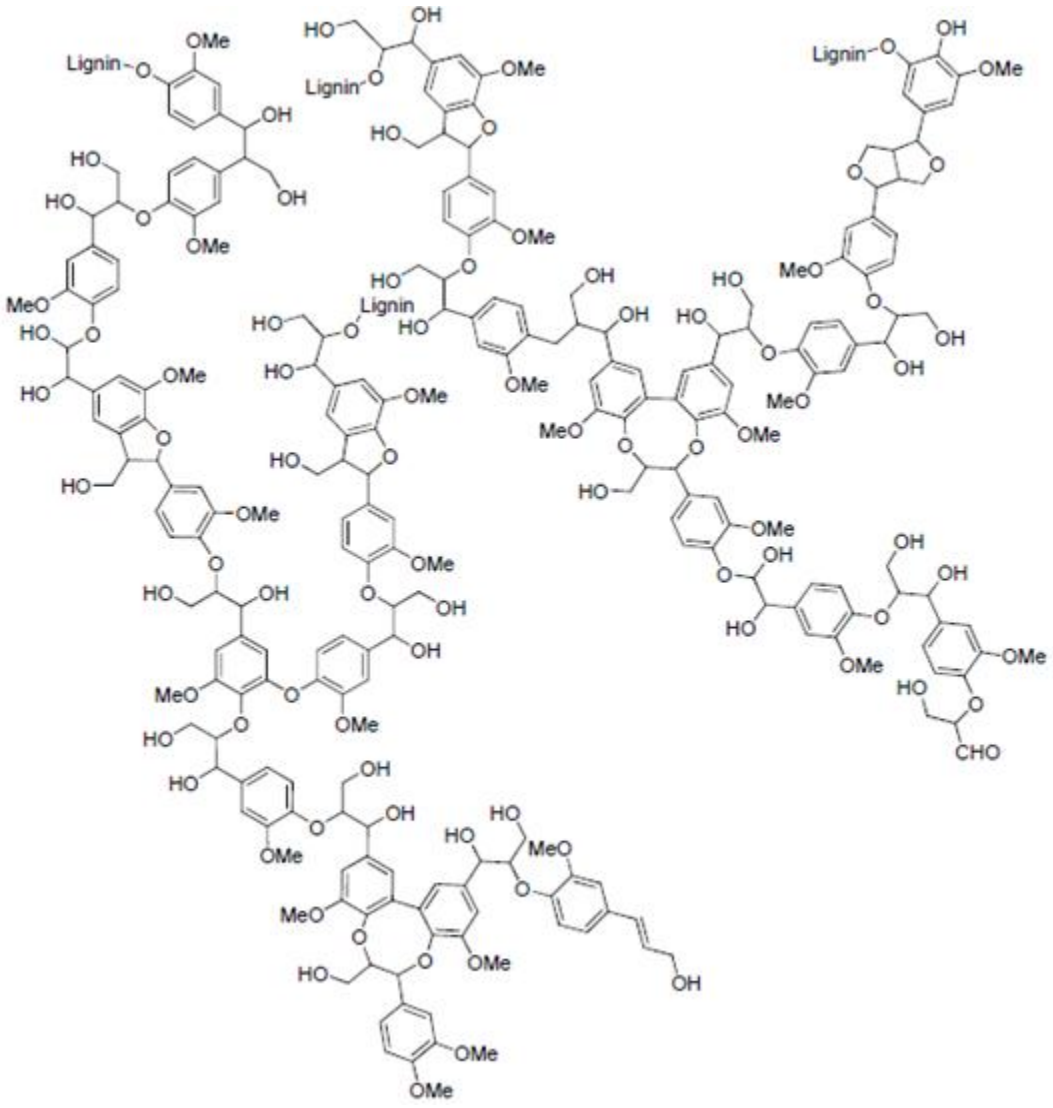

Figure 1.2.1 Softwood lignin [25, 26]

Though there is still ambiguity in lignin's structure, it is well accepted that lignin results from the oxidative radical coupling of basic phenylpropanoid units (Figure 1.2.2) by the action of peroxidases and laccases in plants through the shikmic acid pathway [27-29]. The proportions of the structures vary depending on the biomass type. For example, softwoods (gymnosperms) only consist of coniferyl alcohol-derived constituents and hardwoods (angiosperms) consist of both syringyl and coniferyl structures [30].

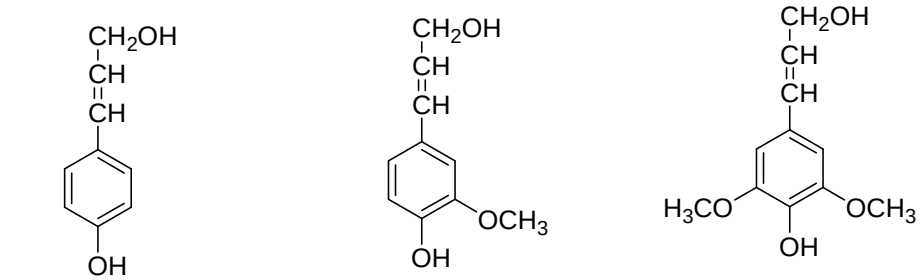

Figure 1.2.2 Lignin monomeric units [30]

The combinatorial-like coupling of monolignols gives rise to a vast and complicated network of inter-unit linkages, mainly of the C-C and C-O type [30]. Figure 1.2.3 shows a general representation of the lignin monomer unit [30]. Table 1.2.1 summarizes the types of linkages commonly found in lignin structures.

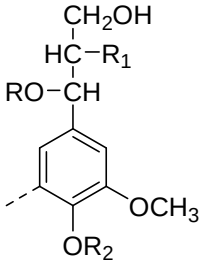

where R=H, alkyl, aryl, alkoxy and aryloxy

Figure 1.2.3 General formula for the phenylpropane unit [30]

Table 1.2.1 Types and frequency of lignin inter-unit linkages in softwood and hardwood [31]

Linkages (per 100 C_9-units)	Softwood (spruce)	Hardwood (beech)
β-O-4	49-51	65
α-O-4	6-8	--
β-5	9-15	6
β-1	2	15
5-5	9.5	2.3
4-O-5	3.5	1.5
β-β	3.5	1.5

Lignin is usually treated by catalytic pyrolysis to convert from solid to liquid phase for further industrial processing [32-34]. Pyrolysis products typically consist of phenolic compounds, acids and water. Exact composition of pyrolysis oil depends on feedstock composition, pyrolysis conditions, residence time and catalyst [35]. Some processes for lignin conversion to aromatic compounds are summarized in Table 1.2.2 [36]. All processes have advantages and disadvantages. The process choice depends on the lignin source and desired products [36].

Table 1.2.2 Processes for lignin valorization into hydrocarbons [36]

Name	Description	State of the art	Pros	Cons
Noguchi Process	Catalytic hydrotreatment of lignin dissolved in a lignin-based phenolic mixture.	Many operating conditions were tested by Crown Zellerbacj company, for the production of phenol and p-cresol, but they were judged nonprofitable in 1965.	High yields in monophenols, coproduction of nonoxygenates.	Expensive reactors for hydrotreatment at > 400 °C, complex separation (distillation) of products.
Catalytic ebullated bed	Lignin is introduced into a CoMo catalyst bed fluidized by boiling phenols, hydrogen being sparged through this ebullated bed. Volatile low oxygen content phenol (mainly cresols) are transferred to the gas phase and are condensed downstream of the bed.	A pilot was operated in 1980.	Mainly phenol and cresol are produced.	A carbonaceous solid is formed and the beds easily clogged.
Base catalyzed depolymerization and HDO of phenols	Lignin is treated by H_2O (catalyzed by NaOH) to yield phenols. The solutions is neutralized and phenols are extracted, and then hydrotreated (50 bar H_2, transition metal catalyst).	In the demonstration stage (Chevron, ENI)	High yield of hydrocarbons (64 wt% dry lignin)	Too many steps to separated phenols from reaction media.
Catalytic Pyrolysis	Lignin is pyrolyzed in presence of a solid catalyst.	Pilots were operated based on FCC units. Many catalysts have been optimized in a pyroprobe (1 mg scale). Researches are conducted to scale up laboratory experiments to a continuous pilot.	No need of hydrogen. Low pressure.	Lignin char is agglomerated with the catalyst, difficult regeneration and steady-state operation.
Pyrolysis, and HDO of condensed pyrolysis vapors	Lignin is pyrolyzed, vapors are condensed and then hydrotreated (100 bar H_2, precious metal catalysts).	A pilot was operated by De Wild et al. (ECN Netherlands). Fluidized-bed clogging happened, but that may be solved by optimizing design.	Phenols are separated from char before catalytic treatment.	Low yield of hydrocarbons heavier than C_6.
Pyrolysis and low pressure, gas phase HDO of uncondensed phenolic vapors	Lignin is pyrolyzed; vapors are hydrotreated before condensation.	After catalyst development with model compounds, experiments focus on real vapors.	Catalysts are not in contact with lignin/char. Easier operation of reactors. Low pressure. Cheap catalyst.	Need the development of a trustable steady-state lignin pyrolysis reactor with a high vapor yield.

1.3 Previous studies on hydrogenation/hydrodeoxygenation of lignin monomeric and dimeric fragments

After pyrolysis, lignin-based liquids need to be treated before use due to their high viscosity, thermal and chemical instability and repolymerization tendency during storage and transportation [37]. A major challenge in the treatment is the removal of oxygen content before lignin fragments can be processed in the petroleum processing infrastructure [38]. The key process for removing oxygen is hydrodeoxygenation (HDO) of the liquid compounds, forming water [39, 40]. Pyrolysis oil model compounds are often used in catalytic hydrodoxygenation studies to evaluate reaction mechanisms and kinetics. Attention has been given mostly to monomeric and dimeric lignin-derived fragments such as phenol, substituted phenols, guaiacol, substituted guaiacols, cresols, and dimers that contain β-O-4 linkages, because of their relatively large percentages in lignin pyrolysis oil. Table 1.3.1 summarizes some major units and their percentages in lignin [41].

Table 1.3.1 Units in lignin [41]

Name	%
Phenol	0.3
2-Methylphenol	0.5
3- and 4-methylphenol	0.8
3-ethylphenol	0.6
guaiacol	1.9
4-methylguaiacol	2.7
syringol	3.1
1,1'-Bis(3,5-dimethoxy-4-hydroxyphenyl)methylene	1.3

Using model compounds such as guaiacol and guaiacol derivatives, numerous hydrodeoxygenation studies have focused on sulfided CoMo and NiMo-based catalysts, which are commonly used commercially for hydrotreatment to remove sulfur, nitrogen and oxygen from petrochemical feedstocks [42-67]. CoMo and NiMo-based catalysts both have been shown to be effective in HDO, where CoMo-based catalysts favor aromatic products and NiMo-based catalysts favor ring-hydrogenated products [66]. However, using sulfided catalysts brings in concerns such about the loss of the sulfided phase during processing and the introduction of sulfur into the product stream [46, 48, 50, 56, 64, 67, 68]. Feeding H_2S with the reactants may help maintain the sulfided phase but it competitively adsorbs with oxygenated compounds and decreases the selectivity towards hydrogenolysis, lowering the production of desired aromatic compounds [67]. Sulfided catalysts also have significant coking issues due to their acidity [46, 51, 52, 62,

69, 70]. Thus, development of non-sulfided catalysts has attracted great interest. Metal nitrides have drawn attention and been shown to be effective in hydrodesulfurization and hydrodenitrogenation [71, 72]. However, reports of their effectiveness in hydrodeoxygenation are limited. Recently, Al_2O_3 supported Mo, W, and V nitride catalysts have been shown to have good activity in HDO of oleic acid and canola oil [73]. Unsupported Mo nitride catalysts also have shown high activity and rapid demethoxylation of guaiacol to phenol [74]. Ni, Fe-based and copper chromite catalysts showed high activity in converting lignin model compounds such as guaiacol to phenols and benzene [41, 75-77]. However, they did not have impressive performance in further hydrogenation of phenols and benzene. On the other hand, noble metals, such as Rh, Pt and Pd-based catalysts have proven effective in producing fully hydrogenated products from lignin monomers [78-80], although the cost of these metals lowers their potential as industrially practical catalysts.

1.4 Objectives

In this study, the conversion of model compounds representing monomeric lignin fragments into cylcohexanols for use as a source of lignin-derived monomers for renewable Nylon 6 production was investigated. Scheme 1.4.1 shows an industrial pathway for the commercial scale conversion from cyclohexanol to Nylon 6. A specific goal of this work is to transform lignin-derived monomeric phenolic species to their cyclohexanol analogs via selective catalytic hydrogenation, for possible use as feedstock for renewable Nylon 6 production. A fixed-bed flow reactor was used to evaluate the selective hydrogenation of individual model phenolic species (guaiacol, 4-methylguaiacol

and diphenyl ether). The catalyst studied was a novel Ni/SiO_2 catalyst developed in our group, which has been shown to form cyclohexanol as an intermediate product starting from phenol [81, 82]. A primary focus was on tuning the reaction conditions to control the hydrogenation and to form desired products, while avoiding the formation of bicyclic species that can be precursors to catalyst deactivation, or fully hydrogenated products of lower value. Based on the product analysis, catalyst compositions and/or reaction conditions that target selective production of cyclohexanol and substituted cyclohexanols will be identified.

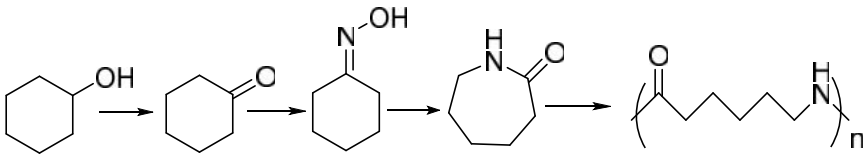

Scheme 1.4.1 Cyclohexanol to Nylon 6

CHAPTER 2

EXPERIMENTAL METHODS

2.1 Materials

The chemicals used in this study, including compounds for catalyst synthesis and pure compounds for GC-FID calibration were obtained from Sigma-Aldrich and used without further purification: nickel (II) nitrate hexahydrate ($Ni(NO_3)_2 \cdot 6H_2O$, 99.999%), tetraethylorthosilicate (TEOS, 98%), poly(ethylene oxide)-block-poly(propylene oxide)-block-poly(ethylene oxide) (PEO-PPO-PEO, avg Mn = 5800), 1,3,5-trimethylbenzene (1,3,5-TMB, 99.0%), hydrochloric acid (HCl, 37%), ammonium hydroxide (NH_4OH, 30%), guaiacol (>98%), phenol (99%), cyclohexanone (99.5%), cyclohexanol (99%), benzene (99.5%), cyclohexane (99%), cyclohexene (99%), 2-methoxycyclohexanol, 2-methoxycyclohexanone (97%), 4-methyguaiacol (97%), p-cresol (99%), 4-methylcyclohexanol (98%), 4-methylcyclohexanone (99%), toluene (99.8%), methylcyclohexane (>99%), 4-methylcatechol (95%), diphenyl ether (>99%), o-cresol (>99%), and silicon carbide (SiC, 200 mesh, 97.5%). The gases used (helium, He, hydrogen, H_2 and 5% oxygen balance helium, 5% O_2 balance He) were of ultra-high purity grade obtained from Air Gas.

2.2 Synthesis of Ni-MCF

Ni-MCF was prepared by hydrothermal synthesis method using $Ni(NO_3)_2 \cdot 6H_2O$ and TEOS as the nickel and silicon sources, respectively. The synthesis procedure was adapted from the work of M. Olarte [82]. The triblock surfactant, PEO-PPO-PEO, was

used as structure directing agent with 1, 3, 5-trimethylbenzene (1, 3, 5-TMB) as the pore expander. The target ratio for the nickel loading was Si/Ni = 12. Two mixtures, A and B, were prepared. Mixture A consisted of 5 g of PEO-PPO-PEO transferred into an Erlenmeyer flask, to which 2.5 g of 1,3,5-TMB and 187.5 g of aqueous HCl of pH = 1.5 were added. The mixture was stirred using a magnetic stir bar at 40°C for about 4 hours. Then mixture B was poured in. Mixture B was prepared by dissolving about 1.23 g $Ni(NO_3)_2 \cdot 6H_2O$ in a stirred flask of 12.5 g of aqueous HCl solution of pH = 1.5 after which 10.625 g of TEOS was then added. Mixture B was stirred for about 2 hours at room temperature before being added to Mixture A. The mixture was then vigorously mixed for 20 hours at 40°C. Then the mixture was cooled and neutralized to pH = 7 by carefully adding drops of NH_4OH (30 wt% NH3) solution. The mixture was then transferred into the Teflon lined autoclaves (*Parr Instruments*, 45 ml) and rotated in the oven for 24 hours at 100°C.

After quenching in an ice bath, the solid contents of the reaction bombs were filtered and washed with copious amounts of water. The solids were then dried overnight in an oven at 85°C. After transferring into porcelain dishes, the solids were calcined to burn off the surfactant template. The calcination protocol consisted of drying the solids under flowing air for 4 hours at 120°C followed by a heating ramp of 1.2 °C/min to 550°C and keeping at 550 °C for 8 hours under flowing air. The solids were then cooled and stored in vials. Before use, the catalyst was pelletized, crushed and sieved. The -35 +70 fraction (average sieve opening = 460 μm) was recovered for use in the catalytic experiments. Another method-wet impregnation-for Ni-MCF synthesis was used to compare with the properties of Ni-MCF made by hydrothermal synthesis. Ni-MCF made by wet-

impregnation was not used in reactions. In wet impregnation synthesis, MCF was first made based on the procedures of Eric Ping et al.'s work [83]: 16.0 g of PEO-PPO-PEO was added into a beaker, followed by the addition of 260 g of DI water and 47.4 g of 37% HCl. The mixture was covered with aluminum foil to limit evaporation and stirred with a large stir bar overnight. Then solution was transferred into a 500 mL Erlenmeyer flask. The mixture was heated to 40 ℃ while being stirred. At the same time, 16.0 g of trimethyl benzene was added to the mixture. Then it was held at 40 ℃ for 2 hours while mixing. After 2 hours 34.6 g of tetraethylorthosilicate was added to the mixture while it was being stirred. After stirring for 5 minutes the solution was placed in oven for 20 hours without stirring. A solution of 184 mg ammonium fluoride and 20 mL water was made and put into the 20-hour-aged solution. The mixture was swirled by hand for 5 minutes before putting into the over at 100 ℃ for 24 hours. After removed out of oven, the mixture was filtered and washed with copious amount of water. Then it was dried in oven overnight at 75 ℃. The solid was calcined at 550 ℃ for 8 hours, using the same calcination protocol in hydrothermal synthesis. 3.3 g of $Ni(NO_3)_2 \cdot 6H_2O$ was dissolved in 5 mL ethanol. The solution was mixed with calcined MCF and dried in oven at 85 ℃ overnight. Then the same calcination protocol was performed again for wet-impregnated Ni-MCF.

2.3 Catalyst characterization

2.3.1 Elemental analysis

Elemental analysis of the catalysts was done by an outside laboratory (Columbia

Analytical Services, Arizona) using ICP-MS analysis. The target molar Si/Ni ratio for the catalysts was 12.

2.3.2 Temperature-programmed reduction (TPR)

Temperature-programmed reduction (TPR) was performed in flowing 10% H_2/Ar with a heating rate of 5 K/min after pre-treating the sample at 200°C in flowing Ar for an hour. After reaching the maximum temperature of 800 °C, the sample was held for 1 hour before cooling. The experiment was carried out using a Micromeritics Autochem II system equipped with a TCD detector. About 0.050g of catalyst was loaded into the quartz U-tube sample holder for each experiment.

2.3.3 Nitrogen physisorption

Nitrogen physisorption experiments on the Ni-MCF at 77 K were carried out using a MicromeriticsTriStar II. Prior to the analysis, the samples (~100 mg) were first degassed overnight at180°C under about 5 mm Hg of total pressure. The surface area was calculated using the Brunauer-Emmett-Teller (BET) equation and the pore size was calculated using Frenkel–Halsey–Hill modified Broekhof–de Boer method (BdB-FHH).

2.3.4 X-ray absorption spectroscopy

Extended X-ray Absorption Fine Structure (EXAFS) and X-ray Absorption Near Edge Structure (XANES) measurements of the reduced and spent (with 4-methylguaiacol) Ni-MCF were conducted at Brookhaven National Laboratory. Reduction and passivation of catalyst were done prior to analysis. Fresh catalyst (~ 100mg) was

reduced ex-situ at 600 °C in100% hydrogen with flow rate of 50 mL/min for 1 hour. After reduction, the catalyst was passivated in 5% oxygen with the balance helium with a flow rate of 10 mL/min at 25 °C for 5 hours before exposure to air. The spent catalyst was collected after the 4-methylguaiacol reaction at WHSV of 10 hr^{-1} and used as is.

XAS analysis was carried out by Dr. Mike Morrill. The spectra were obtained in about 10 min in step-scan, transition mode. Measurements of Ni foil for energy calibration were taken simultaneously with the samples. The 0.5 x 0.5 mm X-ray beam went through Kapton windows at the end of the reactor. Each sample was positioned such that the beam would pass through the center of each sample. The data were fit using the WinXAS 3.1 software. Experimental Ni-O and Ni-Ni phase and amplitude functions were obtained from NiO and Ni foil, respectively, as standards. XANES spectral fits were obtained by a linear combination of the starting catalysts and Ni foil. The edge position was also compared to the XANES spectrum of NiO.

2.3.5 X-ray diffraction

Before analysis with X-ray powder diffraction (XRD), unreacted Ni-MCF was reduced and passivated as described in Section 2.3.4. Spent catalysts were collected after guaiacol, 4-methylguaiacol and diphenyl ether reactions, all at WHSV of 10 hr^{-1}, and used as is. XRD data were taken using a PANalytical X'pert Pro Diffractometer with a Cu-Kα source (λ= 1.5418740 Å) from 2θ = 30° – 65° with a step size of 0.017°. The nickel oxide phase was confirmed by comparing with patterns available in the literature.

2.3.5 Transmission electron microscopy

Transmission electron microscopy (TEM) of fresh and reduced/passivated Ni-MCF was carried out by Dr. Megan Lydon using JEOL 100CX II transmission electron microscope under 100 kV.

2.4 Fixed bed reactor

Figure 2.4.1 shows the flow reactor system. The flow system consisted of the liquid delivery module, the gas delivery module, the down-flow reactor, and the analysis unit. Liquid feed (guaiacol, 4-methylguaiacol or diphenyl ether) was pumped into the flow reactor using a Shimadzu HPLC pump. Flow rates ranged from 0.0078 ml/min to 0.0156 ml/min. Pump pressure ranged between 5.0 and 7.0 MPa at a steady flow rate. Pressure readings outside this range for extended periods signaled a check of the pump was needed for air bubbles, blockages, or other obstructions. Brooks mass flow controllers were used to meter ultra-high purity He and H_2 into the system. During a typical reaction, about 50 ml/min of H_2 and 50 mL/min He were allowed to flow through the system. Helium was used as a purge gas at the end of the reaction for 30 minutes before the reactor and furnace were cooled down to ensure adequate venting of reactants and products out of the system. The reactor was a down flow packed bed column consisting of ¼" stainless steel tube with an internal diameter of 0.152" and length of 24". VCR fittings were welded for connections to the rest of the system at both ends. Silicon carbide was used to disperse the catalyst as well as to promote temperature homogeneity throughout the reactor. The catalyst bed was prepared by mixing the pre-weighed catalyst pellets (-35 +70 fraction) with silicon carbide to obtain a 2 ml mixture. The reactor was brought to the target temperature by an electric furnace. The furnace had three heating zones to allow better temperature control. Temperatures were measured by K-thermocouples, which were then

connected to Omega DPCNi16 PID temperature controllers. The catalyst bed was located at about 14.5” from the top of the reactor. The pressure in the reactor was controlled by a stainless steel needle valve that could stand temperatures up to 500 °C and pressure up to 2000 PSI. Downstream of the reactor were 1/4” lines wrapped with heat tape to keep the reactants and products from condensing and accumulating in the lines. Heated 1/16” lines were connected to the end of the 1/4” lines and led into an online dual detector GC (Agilent 7890A) for on-line analysis of the reaction products. Six-port valves with 0.25 ml sampling loops introduced the products into parallel columns: (1) HP-1ms column to the flame ionization detector (FID); and, (2) HP-PLOT S column to the thermal conductivity detector (TCD). Standard compounds were injected to identify elution times and generate calibration curves for quantification. The excess gas products were passed through a condenser (0°C) with an attached collector. Condensed liquid samples were collected and analyzed in an off-line GC-MS (Shimadzu QP-2010) for the identification of products.

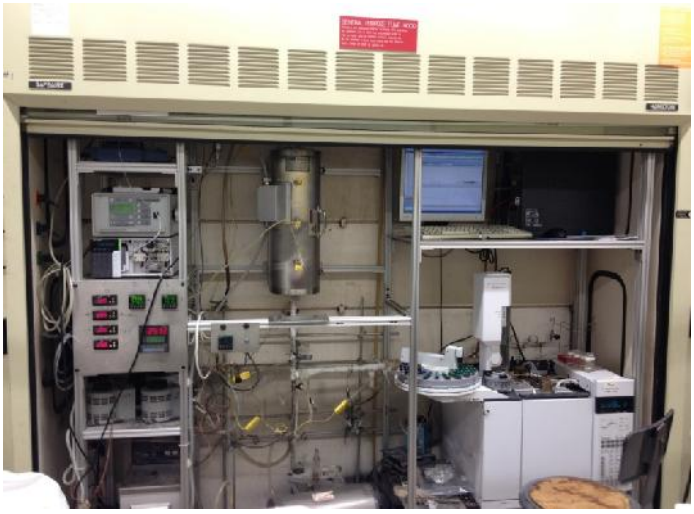

Figure 2.4.1 Reactor system set-up

2.5 Reaction conditions

Flow experiments for all three reactants (guaiacol, 4-methylguaiacol and diphenyl ether) were done at 300°C and at 7.8 bars (100 psig) of the mixture of H_2 and He. The H_2 and He flow rates for all reactions were each set at 50 mL/min. The weight hourly space velocity (WHSV) was determined by the g per hour of reactant fed into the reactor per g of catalyst. WHSV was varied from 10 hr^{-1} to 200 hr^{-1}. The catalyst loading was varied from 10 mg to 50 mg. The liquid reactant flow rate was set at 0.0078 mL/min to 0.0156 mL/min.

CHAPTER 3

RESULTS AND DISCUSSION

3.1 Catalyst characterization

After calcination, fresh Ni-MCF and reduced and passivated Ni-MCF were characterized by N_2 physisorption, XAS, XRD and TEM to elucidate catalyst structural properties.

3. 1. 1 Textural properties

The composition of the Ni-MCF catalysts, surface areas, and pore volumes are summarized in Table 3.1.1.1.

Table 3.1.1.1 Summary of Ni-MCF textural properties

	Target Ni/Si ratio	Actual Ni/Si ratio	BET surface area (m^2/g)	BdB-FHH Pore volume (cm^3/g)
Ni-MCF	1/12	1/11.5	418	1.52

3.1.2 Temperature-programmed reduction (TPR)

To evaluate the reducibility of the catalyst, temperature programmed reduction experiments were conducted. Figure 3.1.2.1 shows the TPR profiles of Ni-MCF and bulk unsupported commercial NiO for comparison.

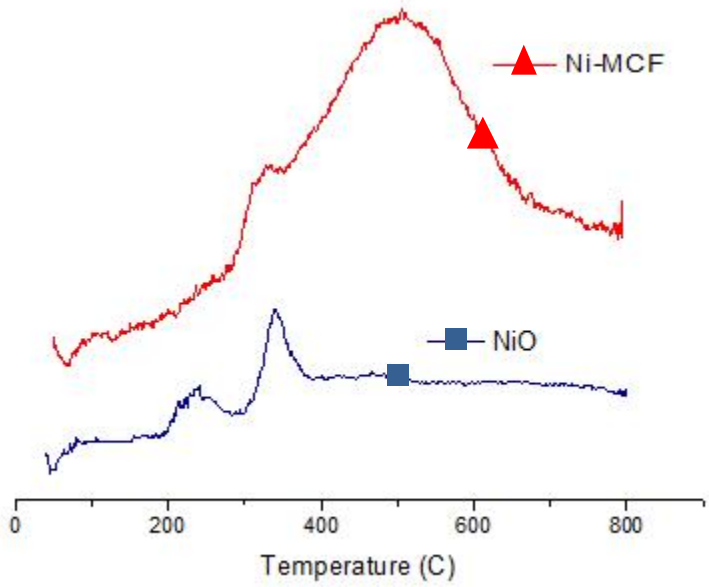

Figure 3.1.2.1 Temperature programmed reduction (TPR) profile of Ni-MCF and standard

Commercial, unsupported NiO showed reduction peaks at 240 ℃ and 340 ℃. The peak at 340 ℃ in NiO corresponds to the majority of the Ni^{2+} species in NiO while some of the non-stoichiometric nickel oxide, Ni_2O_3, is represented by the lower temperature peak at 240 ℃ [84]. Ni^{3+} species contribute to the black color in the nickel oxide sample, which otherwise would be green with only NiO present [84]. In the supported catalyst, the reduction around 340 ℃ is suggested to correspond to the reduction of NiO particles that have minimal interaction with the support [85, 86].

The TPR curve of the Ni-MCF precatalyst shows that complete reduction for the synthesized material occurred at around 500 ℃, which is a much higher temperature than the bulk NiO. The increased reduction temperature may be attributed to 1) metal oxide - support interactions; 2) dispersion of the metal oxide in the support; 3) the metal oxide particle size [84, 86, 87]. The increase in the reduction temperature and peak breadth of Ni-MCF suggests that NiO particles in the Ni-MCF were well-dispersed in the silica

support [88]. The reduction temperature is similar to what has been reported for nickel silicate materials [89-92], suggesting that the incorporation of nickel in the silicate framework for the hydrothermally synthesized nickel catalysts. The shoulder around 340 °C before the major peak in Ni-MCF suggests that a small fraction of NiO was not dispersed into the framework.

3.1.3 X-ray Absorption Spectroscopy (XAS)

To further elucidate the oxidation state of nickel in Ni-MCF, calcined Ni-MCF was reduced and passivated under the conditions described in Section 2.3.4 and X-ray absorption spectroscopy was conducted. Figure 3.1.3.1 and Figure 3.1.3.2 show the k^2-weighted extended X-ray fine absorption structure (EXAFS) and X-ray absorption near edge structure (XANES) spectra of reduced and passivated Ni-MCF with NiO and Ni foil references.

The EXAFS spectrum shows that the Ni-MCF sample was not fully reduced. The Ni-MCF shells show character that corresponds to Ni-O, Ni-O-Ni and Ni-Ni bonding. The lower peak amplitudes indicate well dispersed Ni^{2+} and Ni(0) in the Ni-MCF. The nickel oxide character in reduced Ni-MCF are suggestive of 1) a small particle size, which makes it easy to show character of the layer of NiO outside a Ni metal particle due to passivation; 2) incorporation of Ni species into the support framework forming nickel silicates, which required harsher reduction conditions [91, 92].

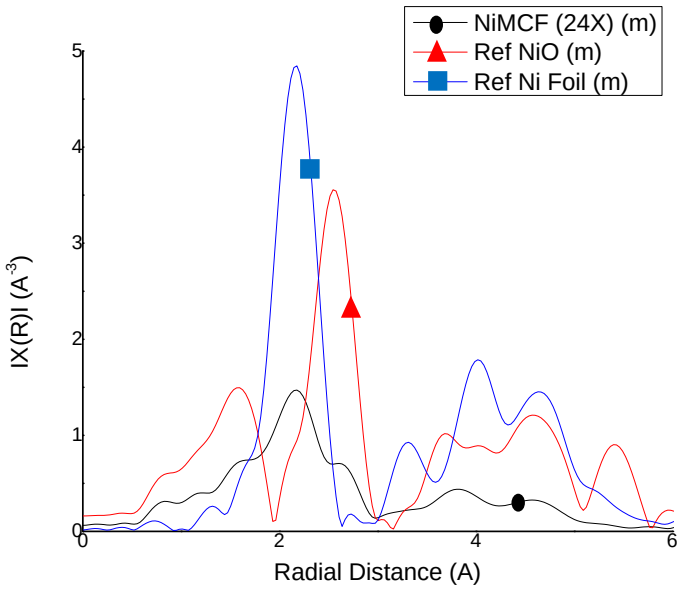

Figure 3.1.3.1 Extended X-Ray absorption fine structure of reduced Ni-MCF with NiO and Ni foil references

XANES spectra of Ni-MCF, in agreement with the EXAFS spectra, show both Ni-Ni and Ni-O character. While the spectrum of Ni foil remained below the white line and that of NiO had a significant intensity well above it, Ni-MCF had its peak maximum in between the two; it had intensity above the white line but not as much as that of NiO. This suggests the presence of unreduced Ni-O in Ni-MCF, albeit less than that in the NiO standard.

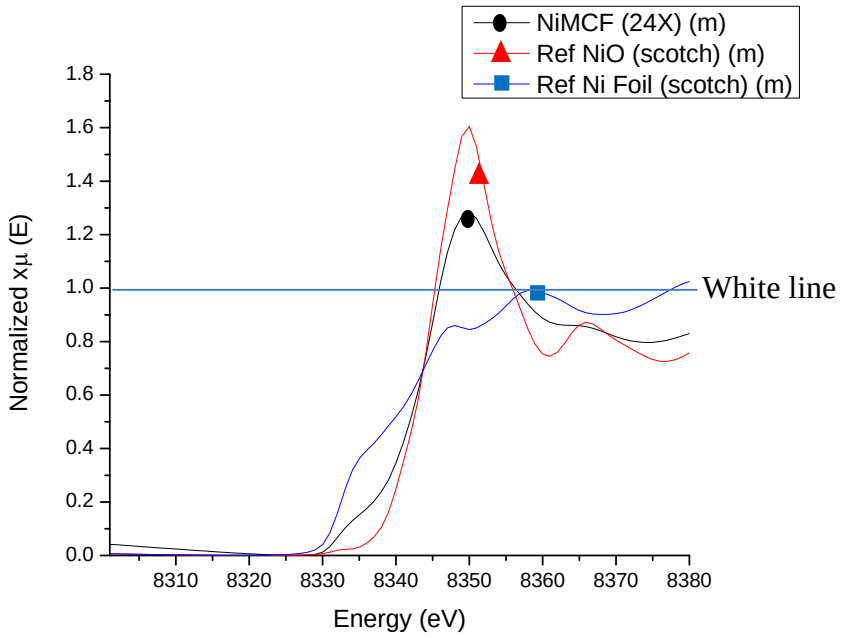

Figure 3.1.3.2 X-ray absorption near edge structure of reduced Ni-MCF with NiO and Ni foil references

3.1.4 X-ray diffraction (XRD)

X-ray diffraction was used to identify the crystalline phase of the nickel formed in the reduced and passivated supported catalyst. Figure 3.1.4.1 shows the diffraction patterns for Ni-MCF. In the reduced Ni-MCF, the main diffraction peaks associated with NiO are 2θ = 34° and 38° [93, 94], and a peak associated with Ni metal is at 2θ = 44.5° [93, 94]. The patterns also show that there were peaks associated with nickel phyllosilicate, which are at 2θ = 35° and 60° [95]. There are two types of Ni phyllosilicate: 2:1 Ni phyllosilicate, whose structural formula is $Si_4Ni_3O_{10}(OH)_2$, and 1:1 Ni phyllosilicate whose structural is $Si_2Ni_3O_5(OH)_4$ [12]. According to Tanaka et al., Ni phyllosilicate is easy to form on porous silica during hydrothermal synthesis [96]. With the synthesis conditions used in this experiment, the dominant structure of the Ni phyllosilicate formed should be the 1:1 Ni phyllosilicate, which was confirmed by the XRD peak at 35°[95,

96]. The following section visually shows the structures of the Ni particles and the mesoporous support.

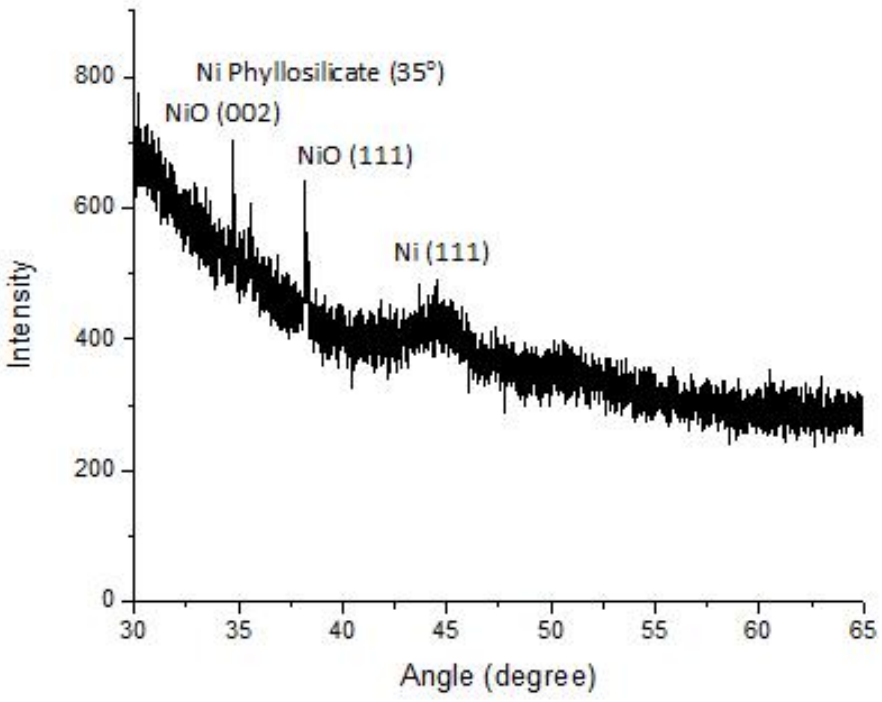

Figure 3.1.4.1 XRD of reduced and passivated Ni-MCF

3.1.5 Transmission electron microscopy

In Figure 3.1.5.1.a and b, the mesoporous silica support structure and Ni particle shape and size for reduced and non-reduced Ni-MCF can be observed. There are Ni particles with needle-like shapes on the support edge in both the reduced and un-reduced catalysts. This shape matches that of Ni phyllosilicate domains reported in the literature [95]. Thus, the TEM images strongly suggest the formation of Ni phyllosilicate on the catalyst support edge in some samples. By comparing the TEM images of hydrothermally synthesized Ni-MCF with Ni-MCF synthesized by wet impregnation, there are clear

structural differences between the two. No needle-like Ni phyllosilicate domains can be observed in the Ni-MCF prepared by wet-impregnation, whose structure is very similar to that of bare MCF support. Ni phyllosilicate domains are usually formed during precipitation when base is added to the solution [95, 96]. This leads to the formation of Ni phyllosilicate during hydrothermal synthesis rather than wet impregnation, since the latter process does not include a precipitation step.

a. b.

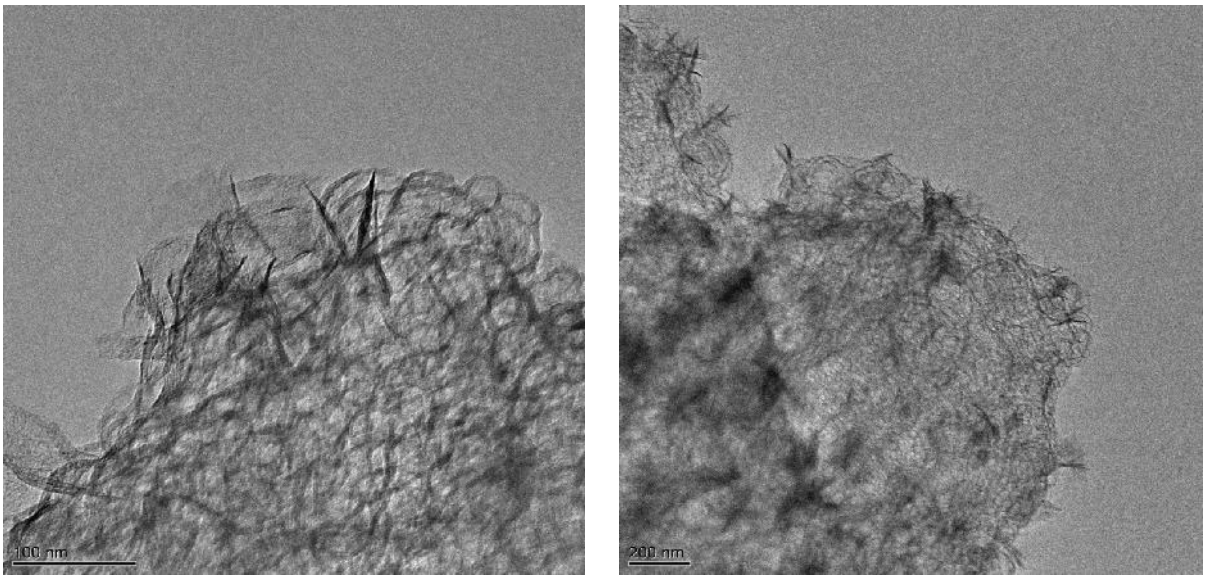

Figure 3.1.5.1 TEM micrographs of (a) reduced Ni-MCF (hydrothermally synthesized); (b) un-reduced Ni-MCF (hydrothermally synthesized)

a.

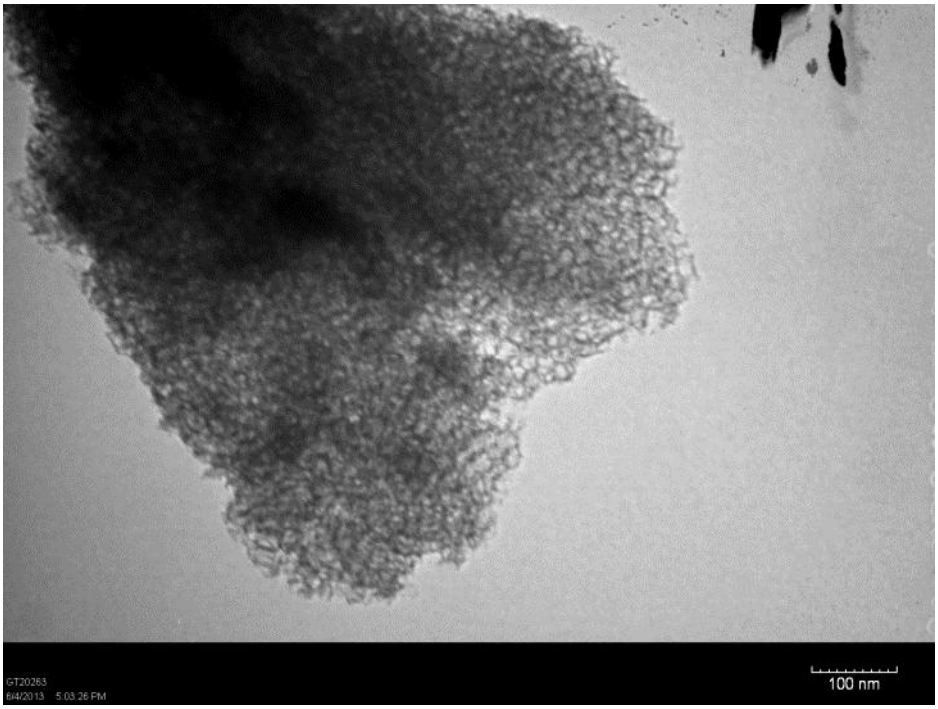

b.

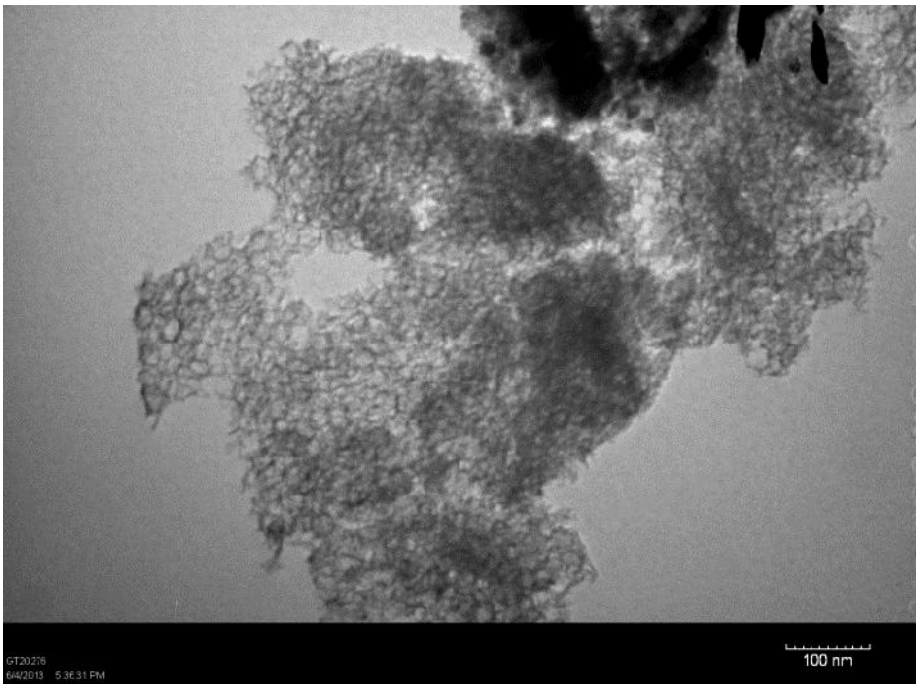

Figure 3.1.5.2 TEM micrographs of (a) bare MCF; (b) un-reduced Ni-MCF (wet impregnation synthesized)

The characterization of the precatalyst reveals the formation of both NiO and Ni phyllosilicate in reduced and passivated hydrothermally synthesized Ni-MCF. XAS spectra and XRD patterns of the reduced and passivated Ni-MCF show the co-existence of Ni oxide and Ni^0 in the material under conditions that closely mirror those likely to occur during catalysis.

3.2 Hydrogenation/hydrodeoxygenation of guaiacol, 4-methylguaiacol and diphenyl ether

3.2.1 Overview of previous study

Among the monomeric and dimeric lignin fragments, guaiacol, 4-methylguaiacol and diphenyl ether were chosen for this study. Guaiacol is of great interest as a bio-oil model compound because of the two representative oxygen containing groups, –OH and –OCH_3. Numerous catalysts such as transition metal-based and noble metal-based catalysts [41-67, 75-80] have been investigated for guaiacol hydrodeoxgenation. Ni-based catalysts have shown good activity for guaiacol conversion and relatively high selectivity towards hydrogenated products such as cyclohexanol and substituted cyclohexanol. Zhao et al. [97] conducted the gas-phase hydrodeoxygenation of guaiacol on catalysts such as Ni_2P/SiO_2, Fe_2P/SiO_2, MoP/SiO_2, Co_2P/SiO_2, and WP/SiO_2. They found that the activities of the catalysts for the HDO of guaiacol followed the order Ni_2P > Co_2P > Fe_2P, WP, MoP.

A guaiacol conversion pathway on Ni-Cu/SiO_2-ZrO_2-La_2O_3 is shown in Scheme 3.2.1.1 [75].

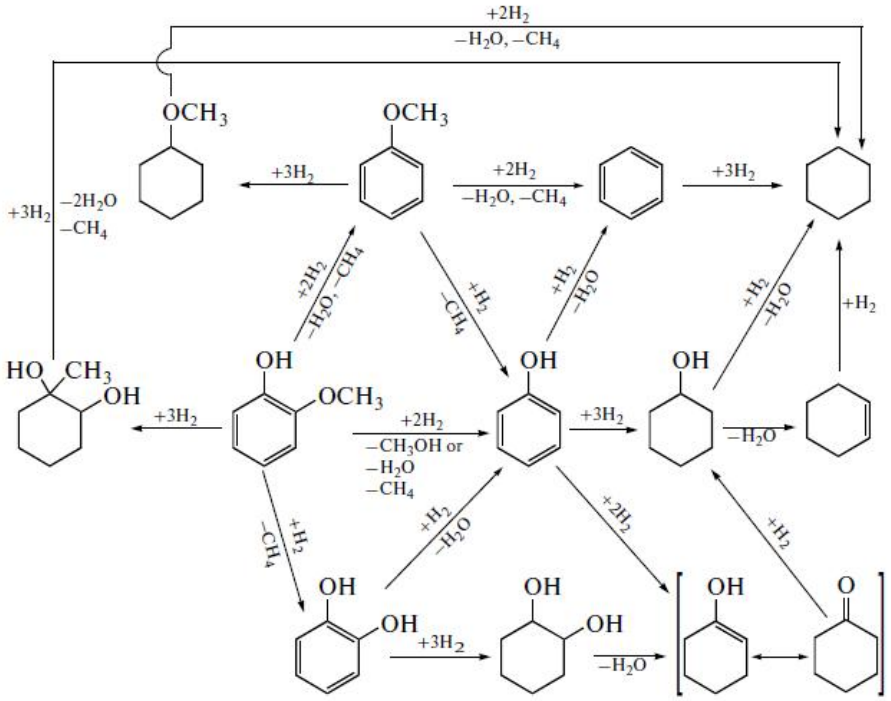

Scheme 3.2.1.1 Pathways of guaiacol conversion over Ni–Cu/SiO_2–ZrO_2–La_2O_3 [75]

The main reaction pathways are 1) demethoxylation to phenol followed by the hydrogenation of the ring to produce cyclohexanol, which can then be converted to cyclohexane; 2) demethylation to catechol followed by the hydrogenation of the ring and dehydration of 1, 2-cyclohexandiol to cyclohexene-1-ol and cyclohexanone [75].

The results from the hydrodeoxygenation of guaiacol at temperatures from 280 ℃ to 360 ℃ and at H_2 pressures of 17 MPa in autoclaves, the conversions and selectivities are shown in Figure 3.2.1.1 and 3.2.1.2 [75].

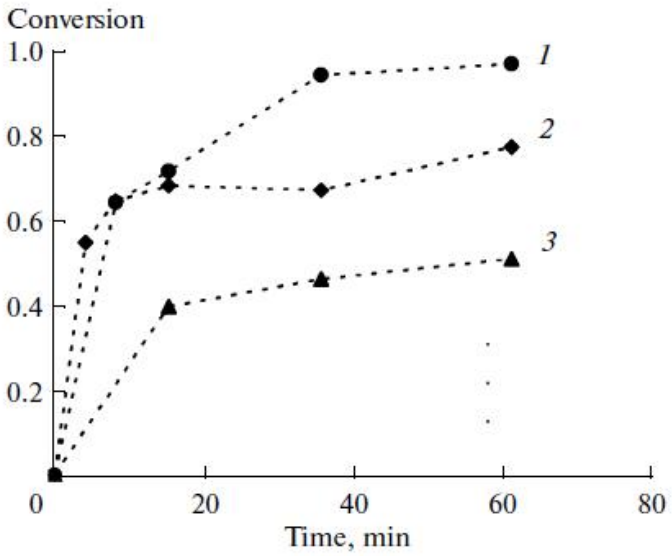

Figure 3.2.1.1 Conversion of guaiacol over Ni–Cu/SiO_2–ZrO_2–La_2O_3 at (1) 280 °C (2) 320 °C (3) 360 °C [75]

Guaiacol conversion decreased with increasing temperature, which may have been due to low gas solubility at high temperature.

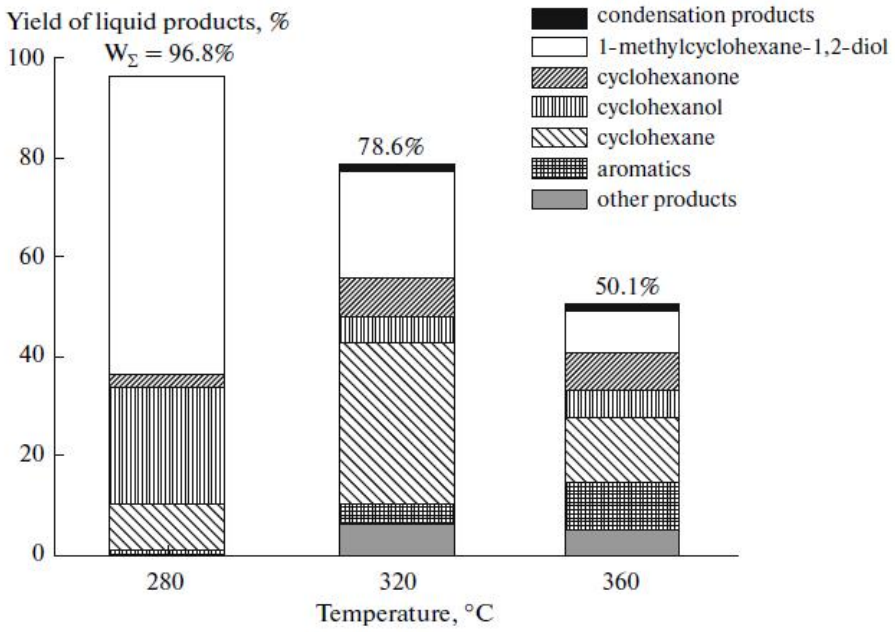

Figure 3.2.1.2 Selectivity of guaiacol conversion products over Ni–Cu/SiO_2–ZrO_2–La_2O_3 [75]

Regarding selectivity, as the temperature was increased, the oxygen containing products, such as 1-methylcyclohexane-1, 2-diol, cyclohexanone and cyclohexanol, selectivity decreased. Meanwhile, the selectivity of the aromatic products and deoxygenation products increased. This suggests that in a certain temperature range the hydrogenolysis of C-O bonds dominates over the hydrogenation of the aromatic ring [75].

A reaction pathway for 4-methylguaiacol conversion is shown in Scheme 3.2.1.2 [98]. The reaction took place at 300 °C and 50 bar of H_2 over a sulfided CoMo-based catalyst in autoclaves. The main reaction products were catechol and *p*-cresol. Since there was no conversion from m-cresol to *p*-cresol under these conditions, *p*-cresol only formed from HDO of methylated aromatics [98]. The pathway shows the lack of hydrogenation ability in the sulfided CoMo catalyst under the conditions used.

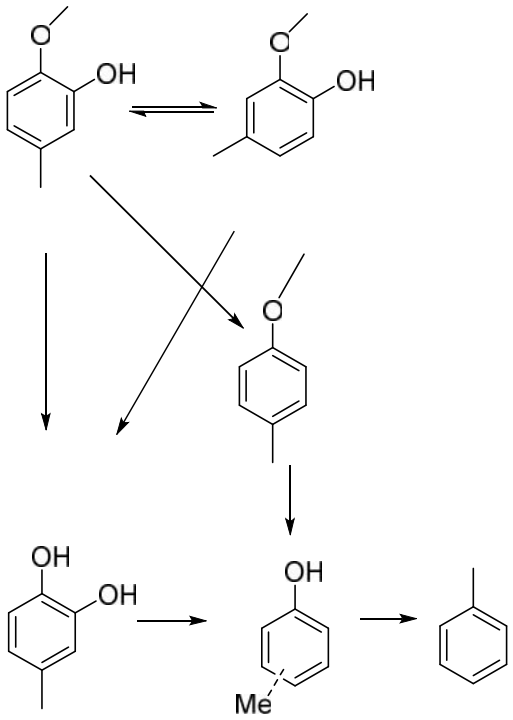

Scheme 3.2.1.2 Pathway of 4-methylguaiacol over sulfided CoMo based catalyst [98]

Diphenyl ether is also a substrate of interest in this study. It was chosen because it has relatively low melting and boiling points among dimeric lignin fragments, which made it feasible for reaction in a flow reactor. Cleavage of the diphenyl ether bond is fairly easy in the presence of Ni-based catalysts and hydrogen. For example, with Raney nickel under 150 atm of H_2 at 150 °C, reaction of diphenyl ether yielded mainly cyclohexane, cyclohexanol and cyclohexyl phenol ether [99] whereas with homogeneous $Ni(COD)_2$ (Bis(1,5-cyclooctadiene)nickel(0)), diphenyl ether was converted to benzene and phenol [100].

With cyclohexanol and substituted cyclohexanols as desired products, a catalyst needs to be developed to hydrogenate aromatic rings without fully hydrogenating the hydroxyl groups, while at the same time minimizing coking and deactivation. Ni was chosen since

it has previously shown good activity for phenol conversion [81, 82] and it is three orders of magnitude cheaper than noble metals, which also showed relatively good conversions of phenol. Mesoporous silica was chosen as the support because of its low acidity, very high specific surface area, controllable pore diameter, narrow pore size distribution and large pore volume. These properties made them more desirable over conventional microporous silica supports, enabling larger molecules to pass through the pores and alleviating transport limitations [101].

3.2.2 Guaiacol conversion in the presence of Ni-MCF

Ni-MCF was tested as a catalyst for guaiacol conversion in a continuous flow reactor at 300 °C and 100 psig total pressure at various WHSVs. The reaction conditions were selected based on extensive trials to ensure the reactant and product mixture could flow smoothly through the reaction system without condensation and clogging of the lines. Also, under the specified conditions the reactions could proceed at quasi steady-state conversions after an initial transient period.

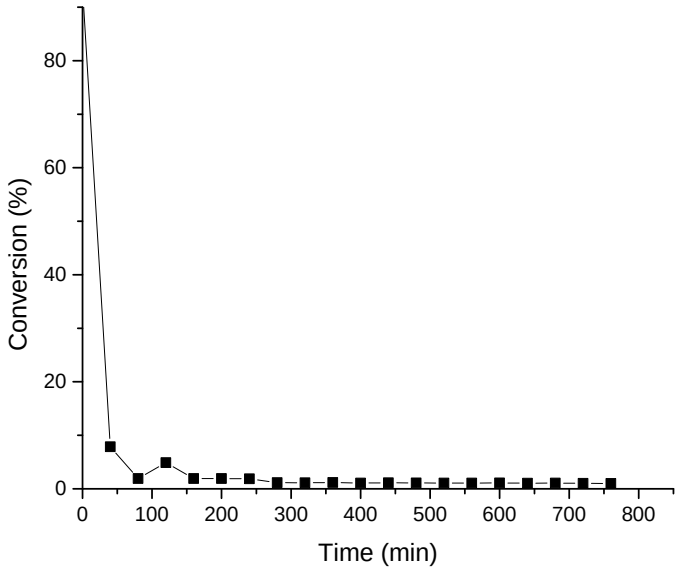

Figure 3.2.2.1 Guaiacol conversion at 300 ^{o}C, 100 psi with Ni-MCF catalyst (10 mg); H_2 flow rate 50 ml/min; WHSV 100 hr^{-1}

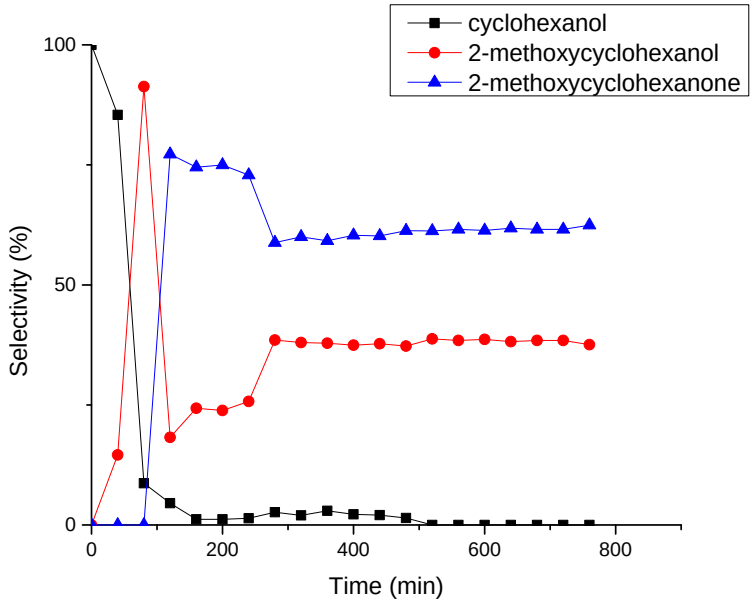

Figure 3.2.2.2 Product selectivities in guaiacol conversion at 300 ^{o}C, 100 psi with Ni-MCF catalyst (10 mg); H_2 flow rate 50 ml/min; WHSV 100 hr^{-1}

At 300 °C, 100 psi and 100 hr^{-1} WHSV, as shown in Figure 3.2.2.1, the guaiacol reaction started at a high conversion of 87%. However, after about 4 hours, the conversion decreased to 1% and stabilized at this value. The sharp conversion drop indicates rapid loss of catalytic activity at high WHSV.

Products obtained in the guaiacol reaction are shown in Figure 3.2.2.2. The initial major product was cyclohexanol, which was the result of guaiacol ring demethoxylation and ring hydrogenation. As the catalyst deactivated, the major products became 2-methoxycyclohexanone and 2-methoxycyclohexanol, which are products from saturation of the aromatic ring in guaiacol. Selectivity for cyclohexanol decreased to 1% at steady-state guaiacol conversion.

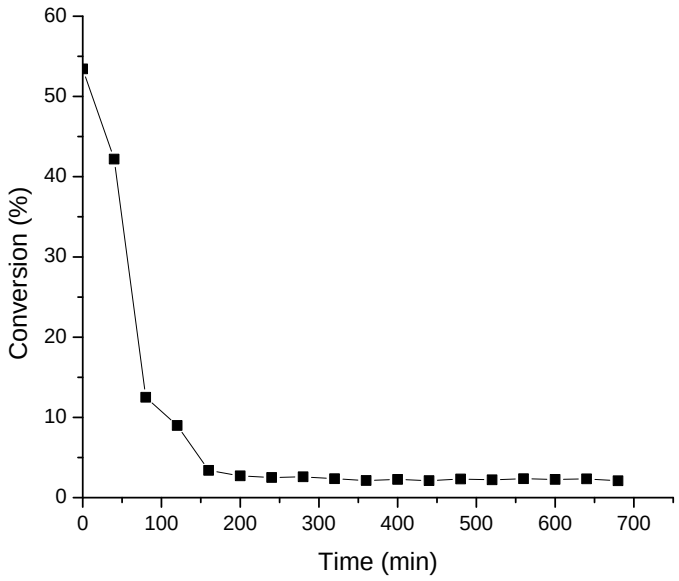

Figure 3.2.2.3 Guaiacol conversion at 300 ^{o}C, 100 psi with Ni-MCF catalyst (10 mg); H_2 flow rate 50 ml/min; WHSV 50 hr^{-1}

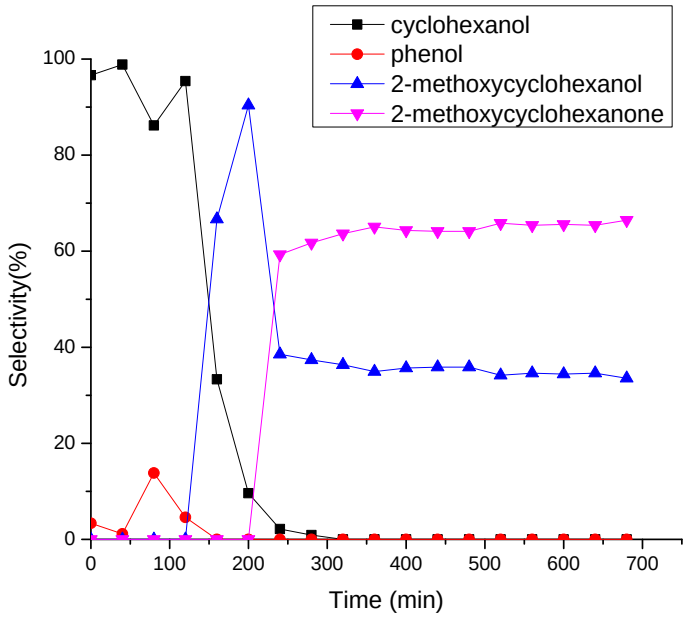

Figure 3.2.2.4 Product selectivities in guaiacol conversion at 300 ^{o}C, 100 psi with Ni-MCF catalyst (10 mg); H_2 flow rate 50 ml/min; WHSV 50 hr^{-1}

In the next reaction, the WHSV was halved by reducing the guaiacol flow rate. At a WHSV of 50 hr^{-1} the initial conversion of guaiacol was around 55% (Figure 3.2.2.3). Conversion decreased again in about 2 hours and reached a steady-state value of 2%.

Products obtained at WHSV of 50 hr^{-1} are shown in Figure 3.2.2.4. The initial major product was cyclohexanol. As conversion decreased, which is an indication of catalyst deactivation, 2-methoxycyclohexanone and 2-methoxycyclohexanol became major products. Selectivity for cyclohexanol decreased to below 1% at steady-state guaiacol conversion, which is similar to the selectivity of cyclohexanol at WHSV of 100 hr^{-1}.

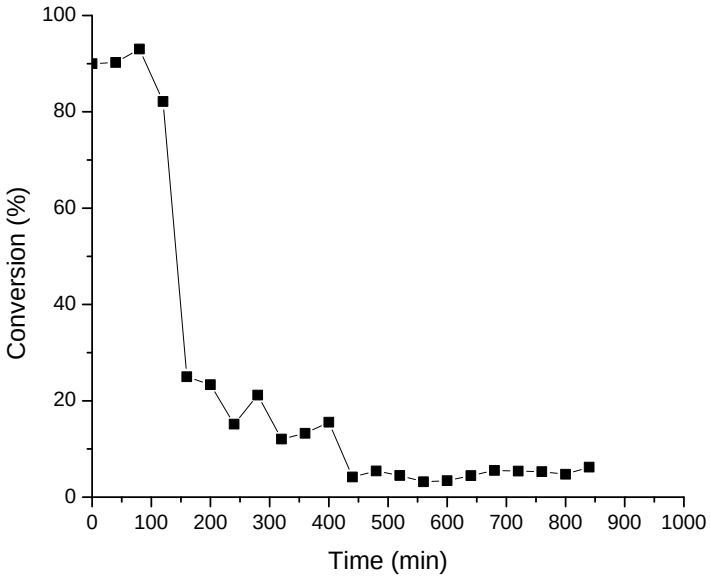

Figure 3.2.2.5 Guaiacol conversion at 300 ^{o}C, 100 psi with Ni-MCF catalyst (20 mg); H_2 flow rate 50 ml/min; WHSV 25 hr^{-1}

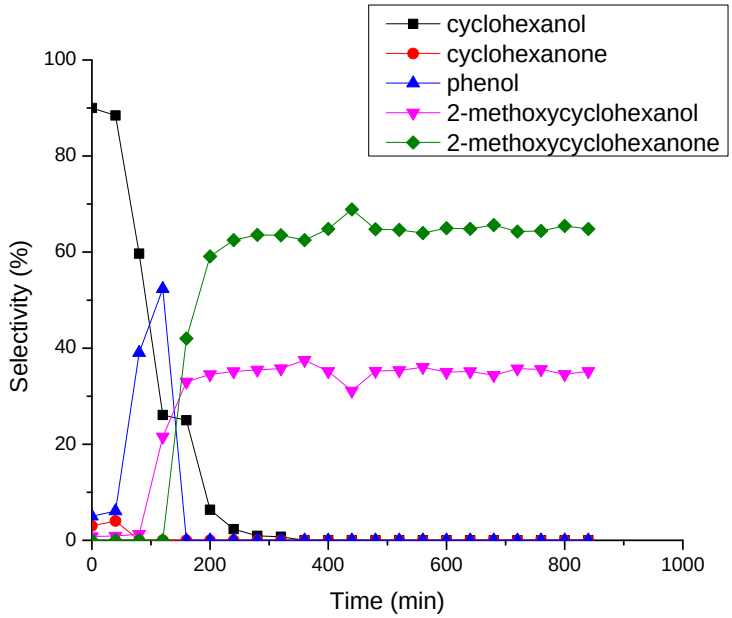

Figure 3.2.2.6 Product selectivities in guaiacol conversion at 300 ^{o}C, 100 psi with Ni-MCF catalyst (20 mg); H_2 flow rate 50 ml/min; WHSV 25 hr^{-1}

In Figure 3.2.2.5, at a WHSV of 25 hr^{-1}, the initial conversion of guaiacol was 90% and remained at 90% for 2 hours. After 2 hours, the conversion decreased to around

20%, indicating fast catalyst deactivation. The conversion was maintained at around 20% for 2 hours, and then gradually decreased to its steady-state value of 5%. The catalyst deactivation was not as rapid as was observed at higher WHSV values of 100 hr^{-1} and 50 hr^{-1}, respectively.

Figure 3.2.2.6 shows the product selectivities at WHSV of 25 hr^{-1}. The initial major product was cyclohexanol. At WHSV of 25 hr^{-1}, a noticeable amount of phenol was formed as the catalyst was deactivating. Essentially no phenol was observed at the WHSV of 100 hr^{-1}, and only a small amount of phenol was observed at the WHSV of 50 hr^{-1}. After catalyst deactivation, major products became 2-methoxycyclohexanone and 2-methoxycyclohexanol. Selectivity for cyclohexanol decreased to below 1% during steady-state conversion.

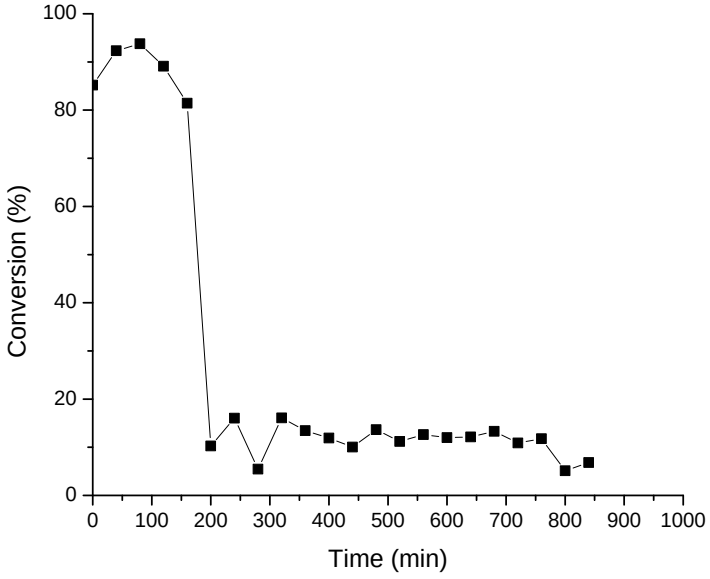

Figure 3.2.2.7 Guaiacol conversion at 300 ^{o}C, 100 psi with Ni-MCF catalyst (30 mg); H_2 flow rate 50 ml/min; WHSV 17 hr^{-1}

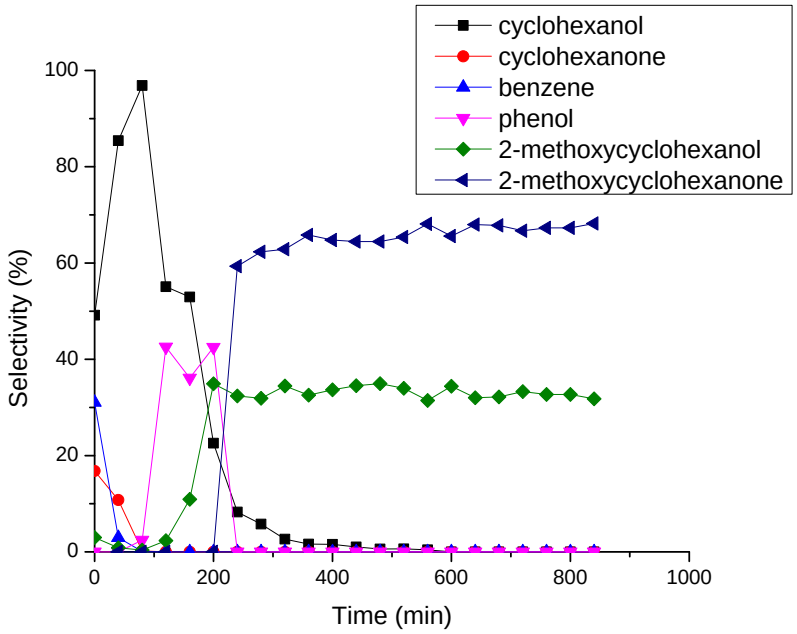

Figure 3.2.2.8 Product selectivities in guaiacol conversion at 300 ^{o}C, 100 psi with Ni-MCF catalyst (30 mg); H_2 flow rate 50 ml/min; WHSV 17 hr^{-1}

Initial conversion of 90% was achieved again at WHSV of 17 hr^{-1}. Deactivation of the catalyst at this WHSV happened over 3 hours. At a WHSV of 17 hr^{-1}, the steady-state conversion was 11% (Figure 3.2.2.7).

The initial major product obtained at a WHSV of 17 hr^{-1} was still cyclohexanol (Figure 3.2.2.8). Other initial products included phenol along with cyclohexanol. Formation of 2-methoxycyclohexanone and 2-methoxycyclohexanol was observed after catalyst deactivation and became the major products at steady-state, while the selectivity of cyclohexanol was below 1%.

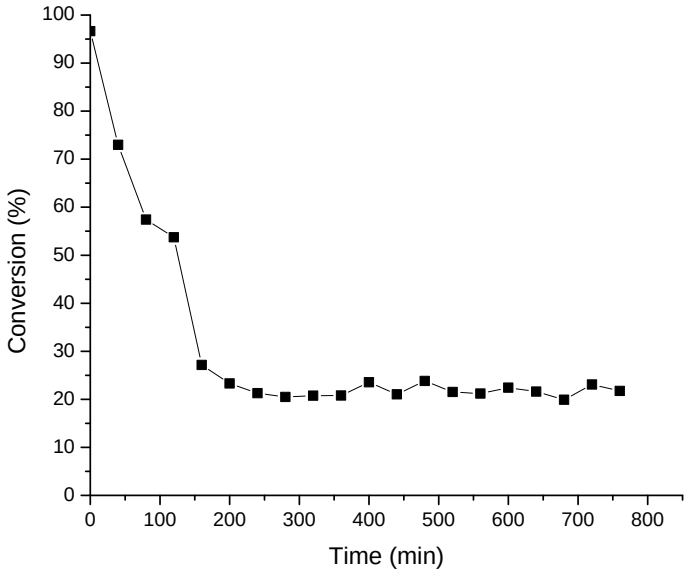

Figure 3.2.2.9 Guaiacol conversion at 300 ^{o}C, 100 psi with Ni-MCF catalyst (50 mg); H_2 flow rate 50 ml/min; WHSV 10 hr^{-1}

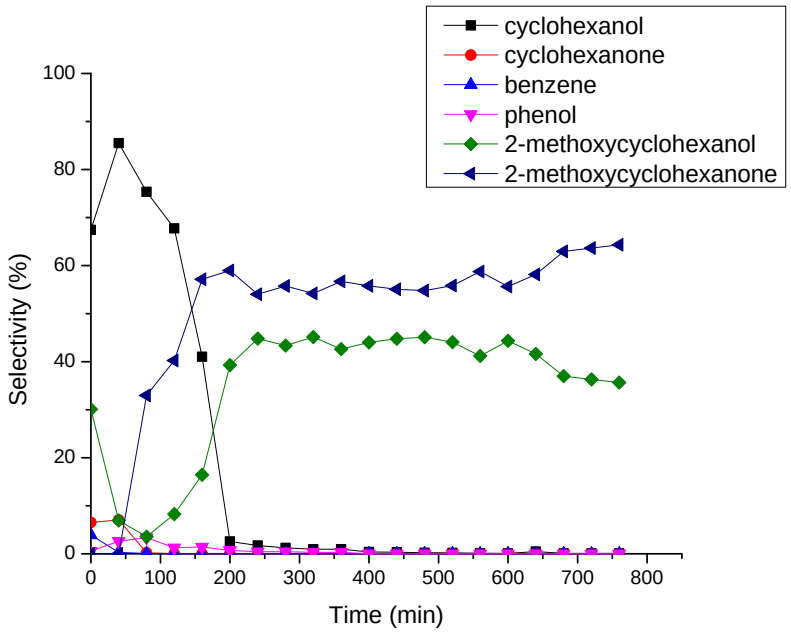

Figure 3.2.2.10 Product selectivities in guaiacol conversion at 300 ^{o}C, 100 psi with Ni-MCF catalyst (50 mg); H_2 flow rate 50 ml/min; WHSV 10 hr^{-1}

At the lowest WHSV used for the guaiacol reactions, 10 hr^{-1}, the initial conversion was 97%. However, as shown in Figure 3.2.2.9, deactivation occurred again and in 3 hours the steady-state conversion became 20%.

Products obtained at WHSV of 10 hr^{-1} are shown in Figure 3.2.2.10. During the initial conversion period the major product was cyclohexanol, while after catalyst deactivation, the major products changed to 2-methoxycyclohexanone and 2-methoxycyclohexanol. The steady-state selectivity of cyclohexanol was less than 1%.

Table 3.2.2.1 Summary of guaiacol conversions and product selectivitys. Reaction conditions: temperature 300 C; pressure, 100 PSI; H_2 flow rate, 50 mL/min; He flow rate, 50 mL/min; catalyst, Ni-MCF; WHSV, 10 hr^{-1}-100 hr^{-1}.

Guaiacol				
WHSV hr^{-1}	Steady-state Major Products	Steady-state Guaiacol conversion %	Selectivity to 2-methoxycyclohexanol %	Initial Major Products
100	2-methoxycyclohexanol; 2-methoxycyclohexanone	1	37	cyclohexanol
50	2-methoxycyclohexanol; 2-methoxycyclohexanone	2	35	cyclohexanol
25	2-methoxycyclohexanol; 2-methoxycyclohexanone	5	35	cyclohexanol
17	2-methoxycyclohexanol; 2-methoxycyclohexanone	11	34	cyclohexanol
10	2-methoxycyclohexanol; 2-methoxycyclohexanone	20	42	cyclohexanol

From the experiments at WHSVs from 10 hr^{-1} to 100 hr^{-1}, it can be concluded that with Ni-MCF as catalyst, guaiacol is mainly converted to highly hydrogenated product-cyclohexanol, which is the target product, but only at the beginning of the reactions. Unfortunately, deactivation was very fast after the reactions started. This is thought to occur by carbon deposition, blocking the catalytic sites so less hydrogen is available on

catalyst surface, decreasing the catalyst's ability to convert 2-methoxycyclohexanol and 2-methoxycyclohexanone to cyclohexanol. As a result, partially hydrogenated products 2-methoxycyclohexanone and 2-methoxycycylohexanol became the major products at steady-state conversions, making up to 99% of the products. These two products reveal that the hydrogenolysis of the methoxy group in guaiacol happens at a slower rate than the hydrogenation of the aromatic ring at steady state conditions. Table 3.2.2.1 summarizes the initial and steady-state products of guaiacol conversions at WHSVs from 10 hr^{-1} to 100 hr^{-1}. There is a clear transition of major products from cyclohexanol to a mixture of 2-methxoycyclohexanone and 2-methoxycyclohexanol for all WHSV studied. As expected, steady-state conversion increased with the decrease of WHSV. Table 3.2.2.1 shows that the steady-state selectivity of 2-methoxycyclohexanol is lower than that of 2-methoxycyclohexanone over the WHSV range from 17 hr^{-1} to 100 hr^{-1}. From WHSV of 17 hr^{-1} to 100 hr^{-1}, the selectivity of 2-methoxycyclohexanol was around 35%, while that of 2-methoxycyclohexanone was around 64%, indicating that hydrogenation of guaiacol to 2-methoxycyclohexanone was favored over it to 2-methoxycyclohexanol at most WHSVs, especially the higher ones. Scheme 3.2.2.1 illustrates proposed reaction pathways of guaiacol. Based on the appearance of each product at different WHSVs, it is clear that guaiacol first undergoes aromatic ring saturation to 2-methoxycyclohexnol and 2-methoxycyclohexanone. Hydrogenolysis of the methoxy group in 2-methoxycyclohexanol happens in the next step and yields cyclohexanol. A route that happens simultaneously is the hydrogenolysis of the methoxy group before saturation of the aromatic ring, which leads to phenol and can be further deoxygenated to benzene and hydrogenated to cyclohexane. However, since the formation of phenol was observed only

at low WHSV values for a short period of time, guaiacol was mainly converted to cyclohexanol through 2-methoxycyclohexanone and 2-methoxycyclohexanol under the conditions of this study at steady state.

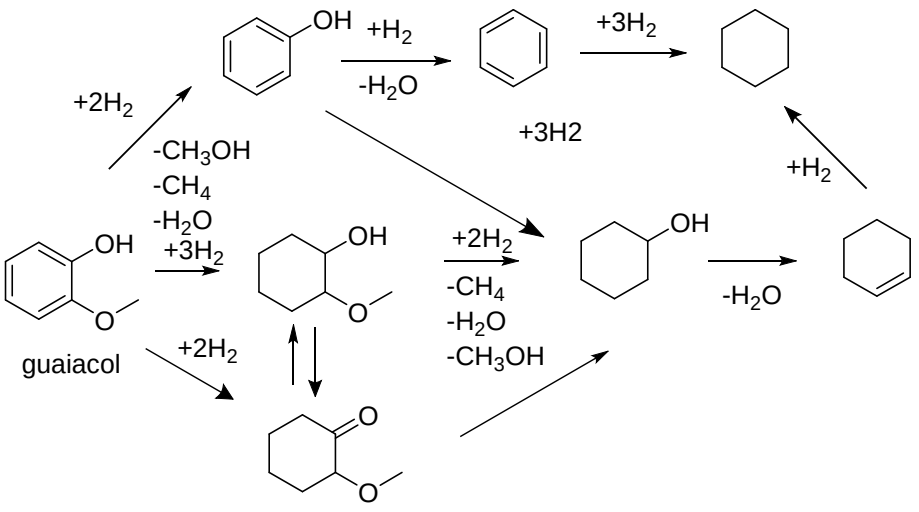

Scheme 3.2.2.1 Reaction pathways of guaiacol on Ni-MCF

3.2.3 4-Methylguaiacol conversion in the presence of Ni-MCF

The second substrate tested was 4-methylguaiacol. The reaction conditions used for 4-methylguaiacol were the same as for guaiacol.

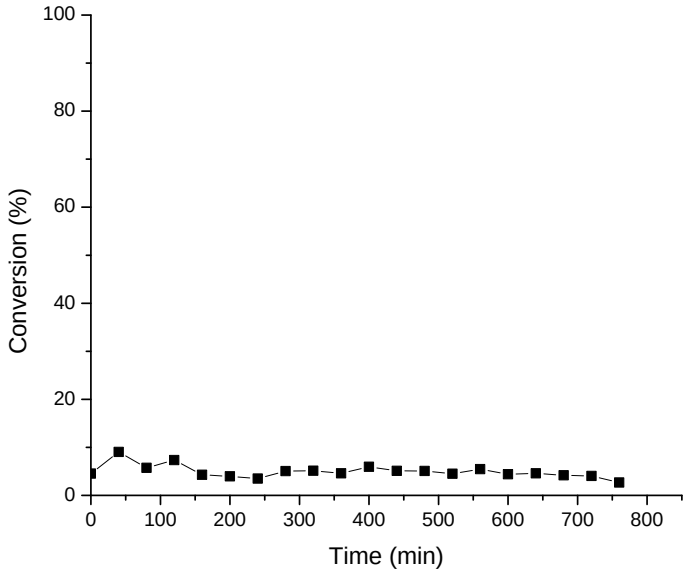

Figure 3.2.3.1 4-methylguaiacol conversion at 300 ^{o}C, 100 psi with Ni-MCF catalyst (10 mg); H_2 flow rate 50 ml/min; WHSV 50 hr^{-1}

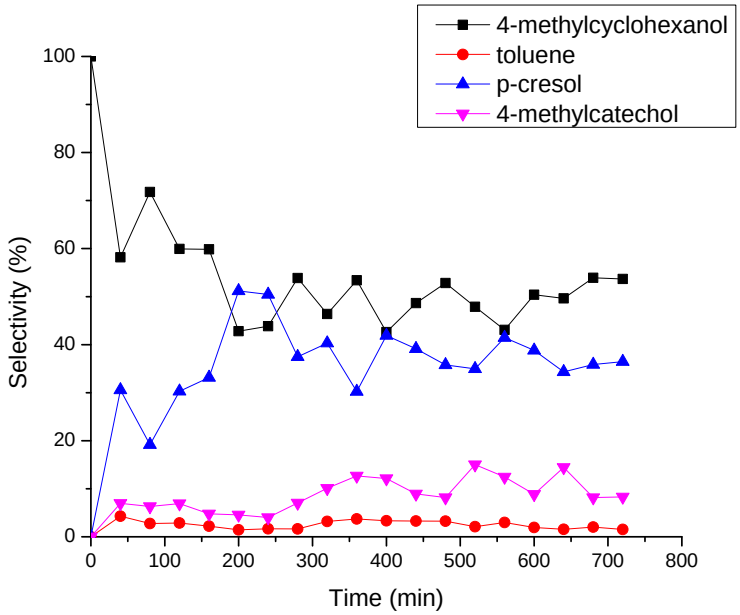

Figure 3.2.3.2 Product selectivities in 4-methylguaiacol conversion at 300 ^{o}C, 100 psi with Ni-MCF catalyst (10 mg); H_2 flow rate 50 ml/min; WHSV 50 hr^{-1}

Figure 3.2.3.1 shows 4-methylguaiacol conversion over 13 hours at WHSV of 50 hr^{-1} at 300 °C and 100 psi. The conversion started at 10%, and stabilized at 5%. There was no significant catalyst deactivation at high WHSV, as the conversion was steady at 5% after 2.5 hours.

Products obtained from the 4-methylguaiacol reaction are shown in Figure 3.2.3.2. The initial major products were 4-methylcyclohexanol and *p*-cresol, which are hydrogenation and hydrogenolysis products of 4-methylguaiacol. In 2 hours the selectivity of 4-methylcyclohexanol decreased to a stable value of 50% while the *p*-cresol selectivity stabilized at ~ 40%, with the rest of the products being 4-methylcatechol and toluene.

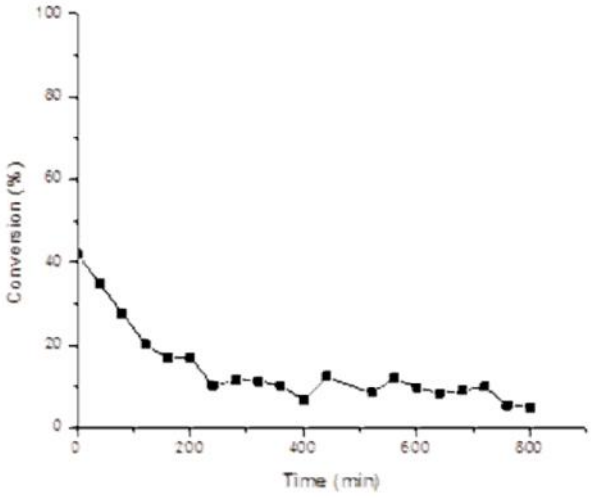

Figure 3.2.3.3 4-methylguaiacol conversion at 300 °C, 100 psi with Ni-MCF catalyst (20 mg); H_2 flow rate 50 ml/min; WHSV 25 hr^{-1}

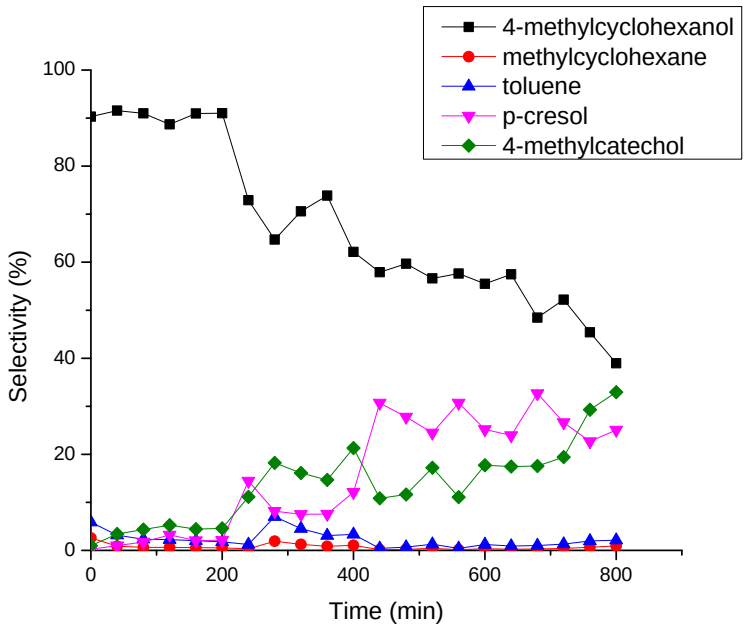

Figure 3.2.3.4 Product selectivities in 4-methylguaiacol conversion at 300 ^{o}C, 100 psi with Ni-MCF catalyst (20 mg); H_2 flow rate 50 ml/min; WHSV 25 hr^{-1}

The conversion of 4-methylguaiacol at a WHSV of 25 hr^{-1} is shown in Figure 3.2.3.3. The conversion started at 40% and stabilized at 10% in 4 hours. At this WHSV, catalyst deactivation became more noticeable.

Figure 3.2.3.4 shows the products obtained in 4-methylguaiacol reaction at WHSV of 25 hr^{-1}. 4-methylcyclohexanol started as the major product at 90% selectivity for 4 hours, which is a period with slow catalyst deactivation. Starting in the 4th hour, the selectivity for 4-methylcyclohexanol began to decrease. The steady-state selectivity of 4-methylcyclohexanol was 50%. On the other hand, the selectivity of p-cresol increased and stabilized at 30%. Another product with increasing selectivity through the reaction was 4-methylcatechol. It had a steady-state selectivity of 18%. Toluene and methylcyclohexane accounted for less than 1% of all products.

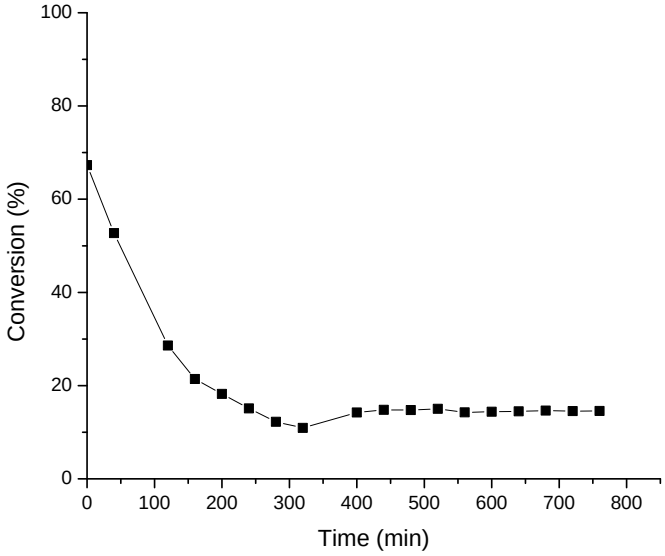

Figure 3.2.3.5 4-methylguaiacol conversion at 300 ^{o}C, 100 psi with Ni-MCF catalyst (30 mg); H_2 flow rate 50 ml/min; WHSV 17 hr^{-1}

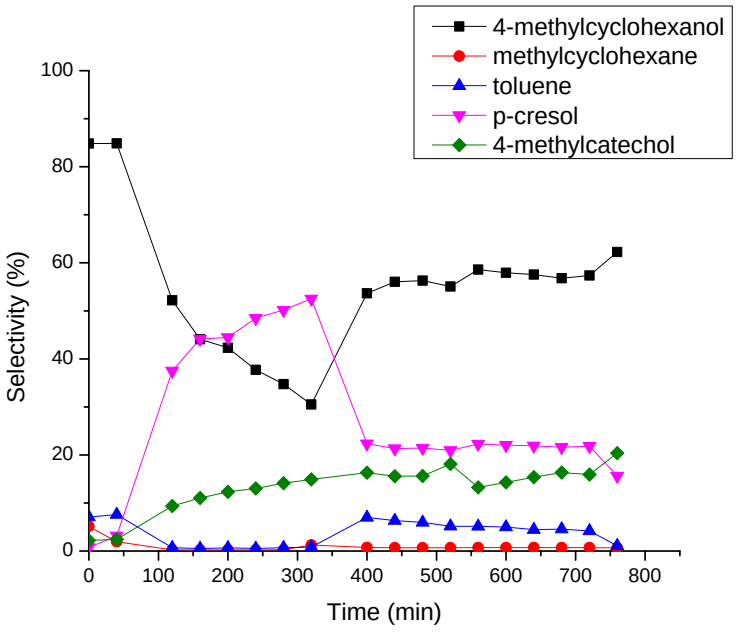

Figure 3.2.3.6 Product selectivities in 4-methylguaiacol conversion at 300 ^{o}C, 100 psi with Ni-MCF catalyst (30 mg); H_2 flow rate 50 ml/min; WHSV 17 hr^{-1}

At a WHSV of 17 hr^{-1}, the initial 4-methylguaiacol conversion was 70%. The conversion gradually decreased to a stable value of 15% within 5 hours. Figure 3.2.3.5 shows that the conversion decreased slower from a reaction time of 150 minutes to 320 minutes than in the period before 150 minutes, suggesting that the catalyst deactivation was faster at the beginning of the reaction, which is consistent with what was observed with guaiacol reaction. Deactivation slowed down as the reactions proceeded, as the rate of carbon deposition likely decreased over time [75].

Products obtained in the 4-methylguaiacol reactions are shown in Figure 3.2.3.6. 4-methylcyclohexanol was the initial main product. Over time, the selectivity for 4-methylcyclohexanol decreased while that of *p*-cresol rose. 4-methylcyclohexanol was likely the hydrogenation product of *p*-cresol. The selectivity change, with less p-cresol converting to 4-methylcyclohexanol over time, indicates catalyst activity loss as the reaction proceeded. For times between 150 minutes and 320 minutes, the selectivity to *p*-cresol was higher than that of 4-methylcyclohexanol. However, the selectivity of *p*-cresol decreased after 320 minutes and stabilized at 25%, while that of 4-methylcatechol stabilized at 20% as the conversion became steady. The steady-state 4-methylcyclohexanol selectivity was 50%.

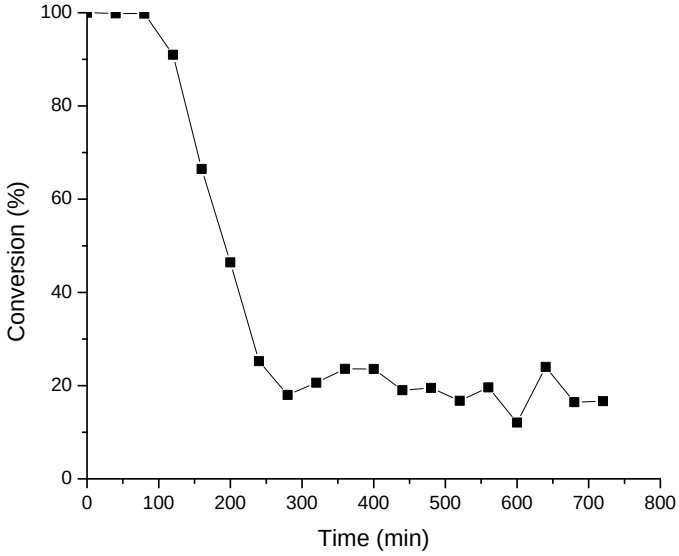

Figure 3.2.3.7 4-methylguaiacol conversion at 300 ^{o}C, 100 psi with Ni-MCF catalyst (40 mg); H_2 flow rate 50 ml/min; WHSV 13 hr^{-1}

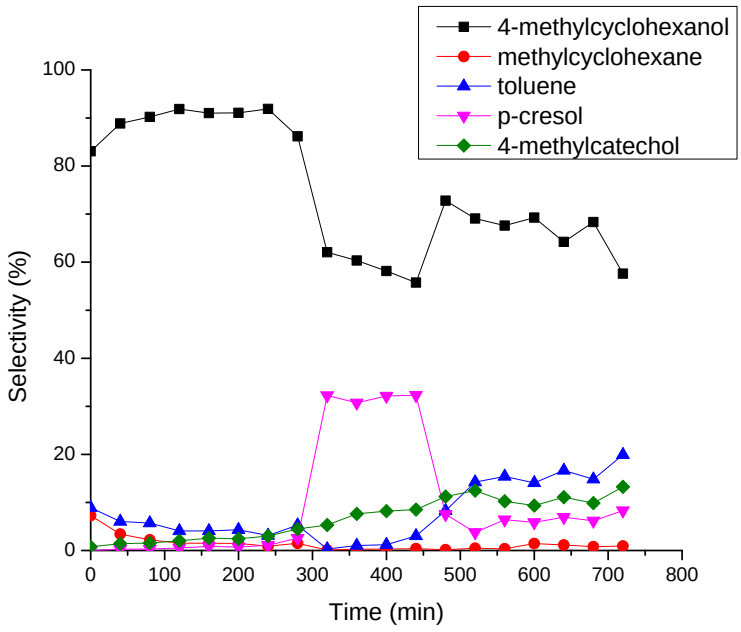

Figure 3.2.3.8 Product selectivities in 4-methylguaiacol conversion at 300 ^{o}C, 100 psi with Ni-MCF catalyst (40 mg); H_2 flow rate 50 ml/min; WHSV 13 hr^{-1}

When WHSV was brought down to 13 hr^{-1}, almost the entire incoming 4-methylguaiacol stream was converted to products (conversion higher than 99%) in the first 2 hours. Then the conversion quickly dropped in 2 hours to a steady-state value of 20%, which indicates fast catalyst deactivation between 3-5 hours.

The dominant product at a WHSV of 13 hr^{-1} at the beginning of the reaction was still 4-methylcyclohexanol (selectivity about 90%). As the reaction conversion became steady, the selectivity to 4-methylcyclohexanol decreased, while that of p-cresol increased. Similar to the reaction at WHSV of 17 hr^{-1}, the selectivity for 4-methylcyclohexanol increased after decreasing, and the trend was opposite for *p*-cresol, showing that *p*-cresol and 4-methylcyclohexanol were linked through the same reaction path. Eventually the selectivities of 4-methylcyclohexanol, *p*-cresol and 4-methylcatechol were stable at 75%, 8% and 10%.

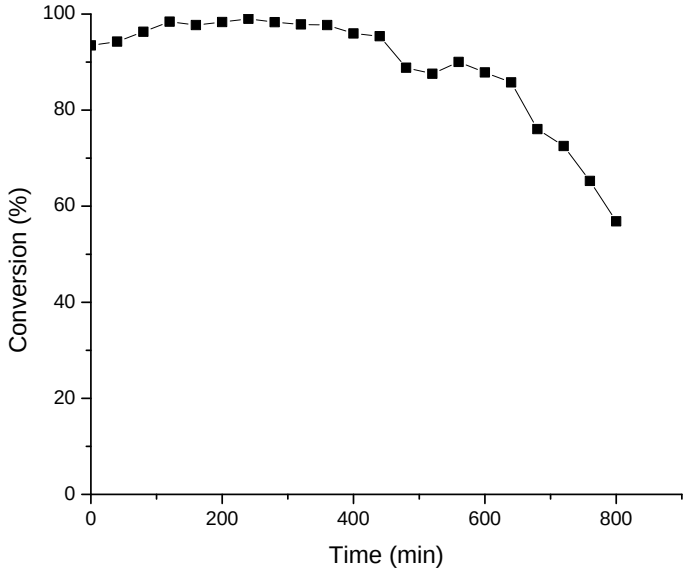

Figure 3.2.3.9 4-methylguaiacol conversion at 300 ^{o}C, 100 psi with Ni-MCF catalyst (50 mg); H_2 flow rate 50 ml/min; WHSV 10 hr^{-1}

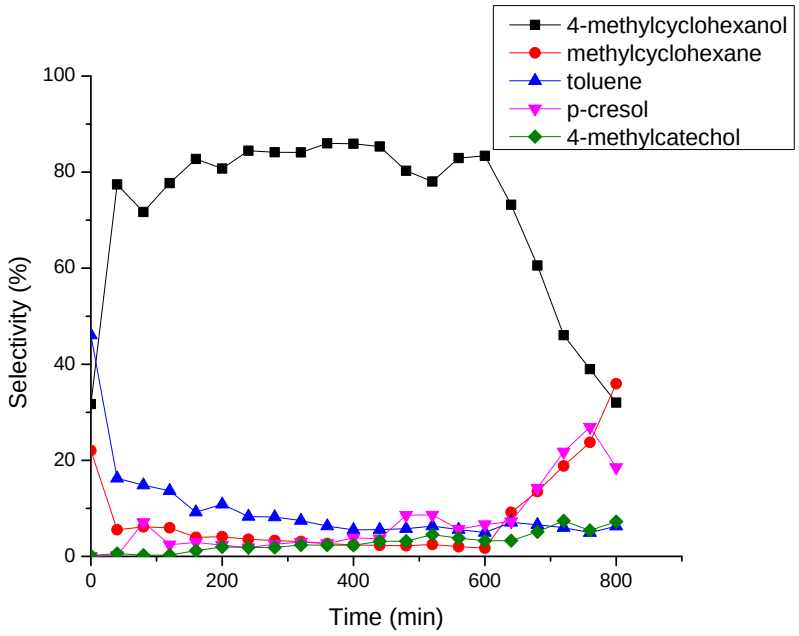

Figure 3.2.3.10 Product selectivities in 4-methylguaiacol conversion at 300 ^{o}C, 100 psi with Ni-MCF catalyst (50 mg); H_2 flow rate 50 ml/min; WHSV 10 hr^{-1}

At a WHSV of 10 hr^{-1}, the conversion started at above 90% and stayed steady at around 95% for 7 hours (Figure 3.2.3.9). The conversion drop, which indicates catalyst deactivation, did not happen until after 7 hours of reaction. The reason for the high conversion through most of the reaction time is possibly the depletion of the reactant. This would mask catalyst deactivation caused by carbon deposition, and still provide nearly complete conversion.

Because of the high catalyst activity, hydrogenation of the aromatic ring in 4-methylguaiacol was the dominant reaction and selectivity for 4-methylcyclohexanol was as high as 80% for nearly 10 hours. After catalyst deactivation, the selectivity of 4-methylcyclohexanol started decreasing and those of p-cresol, 4-methylcatechol and methylcyclohexane increased. It is worth mentioning that the selectivity of methylcyclohexane increased as that of 4-methylcyclohexanol decreased at the end of the

reaction. This could be because the methanol produced from hydrogenolysis of 4-methylguaiacol accumulated on the catalyst surface as the reaction proceeded. Methanol, with pKa of 15 at 300 °C, or the inherent acidity on the catalyst may have promoted the dehydration of 4-methylcyclohexanol to methylcycohexane [98].

Table 3.2.3.1 Summary of 4-methylguaiacol conversions and product selectivitys. Reaction conditions: temperature 300 C; pressure, 100 PSI; H_2 flow rate, 50 mL/min; He flow rate, 50 mL/min; catalyst, Ni-MCF; WHSV, 10 hr^{-1}-50 hr^{-1}.

4-Methylguaiacol

WHSV hr^{-1}	Steady-state Major Products	Steady-state 4-methylGuaiacol conversion %	Selectivity to 4-methylcyclohex-anol	Initial Major Products
50	4-methylcyclohexanol; *p*-cresol	4	48	4-methylcyclohexanol; *p*-cresol
25	4-methylcyclohexanol; *p*-cresol	10	48	4-methylcyclohexanol
17	4-methylcyclohexanol; *p*-cresol	16	55	4-methylcyclohexanol
13	4-methylcyclohexanol; *p*-cresol	22	70	4-methylcyclohexanol
10	4-methylcyclohexanol	95	80	4-methylcyclohexanol

Table 3.2.3.1 summarizes the steady-state conversions of 4-methylguaiacol from WHSV of 10 hr^{-1} to 50 hr^{-1}, as well as the initial and steady-state major product selectivities. 4-methylguaiacol showed high initial conversion with Ni-MCF as the catalyst. The initial product for WHSV from 10 hr^{-1} to 25 hr^{-1} was 4-methylcyclohexanol, and those for WHSV of 50 hr^{-1} were 4-methylcyclohexanol and *p*-cresol. Conversion decreased from WHSV of 13 hr^{-1} to 50 hr^{-1} as the reactions proceeded, which indicates catalyst deactivation. With catalyst deactivation, the major reaction products became a

mixture of 4-methylcyclohexanol and *p*-cresol, resulting from a decrease in hydrogenation ability due to loss of active catalytic sites due to carbon deposition (shown in spent catalyst characterization). The exception is at a WHSV of 10 hr^{-1}, where no obvious conversion decrease was observed until the 12^{th} hour. This means that the catalyst amount was large enough to provide sites for hydrogenation for 12 hours. The steady-state selectivity of 4-methylcyclohexanol kept increasing as the WHSV was lowered, showing that more p-cresol was hydrogenated to 4-methylcyclohexanol with the increase in catalytic sites.

Based on the product selectivity information at different WHSVs, 4-methylguaiacol reaction pathways are proposed in Scheme 3.2.3.1. 4-Methylcatechol, which had steady-state selectivity of between 10% and 20% for all WHSV, is a hydrogenolysis product of 4-methylguaiacol. 4-methylguaiacol is also partially demethoxylated to p-cresol, which can be a dehydration product of 4-methylcatechol as well. *p*-Cresol then undergoes hydrogenation to 4-methylcyclohexanol or dehydration to toluene (to a much lower extent than 4-methylcyclohexanol), showing *p*-cresol is more favorably hydrogenated than dehydrated in the presence of Ni-MCF. 4-methylcyclohexanol can be further dehydrated to 4-methylcyclohexene, which can eventually be hydrogenated to methylcyclohexane. Toluene can also undergo hydrogenation to methylcyclohexane. The methylcyclohexane amounts achieved in the reactions were below 1% at all WHSV, showing the lack of the dehydration/hydrogenation abilities in the final stage.

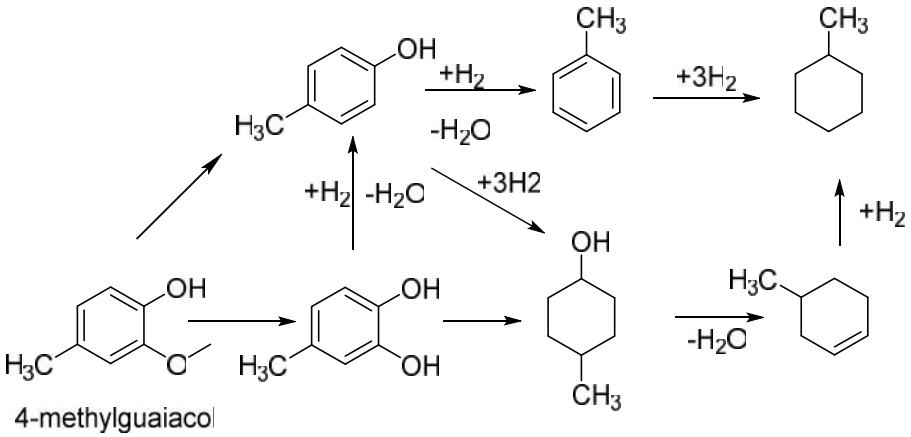

Scheme 3.2.3.1 Reaction pathways of 4-methylguaiacol on Ni-MCF

3.2.4 Diphenyl ether conversion in the presence of Ni-MCF

Lastly, diphenyl ether was used as a substrate to represent dimeric lignin model fragments. The same reaction conditions as for guaiacol and 4-methylguaiacol were used for diphenyl ether. Due to catalyst's high activity for diphenyl ether conversion, higher WHSVs were used to reveal its effect on diphenyl ether conversion.

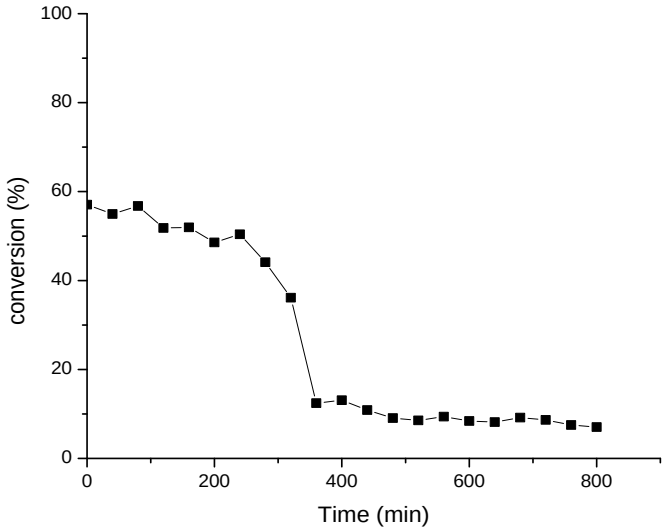

Figure 3.2.4.1 Diphenyl ether conversion at 300 ^{o}C, 100 psi with Ni-MCF catalyst (5 mg); H_2 flowrate 50 ml/min; WHSV 200 hr^{-1}

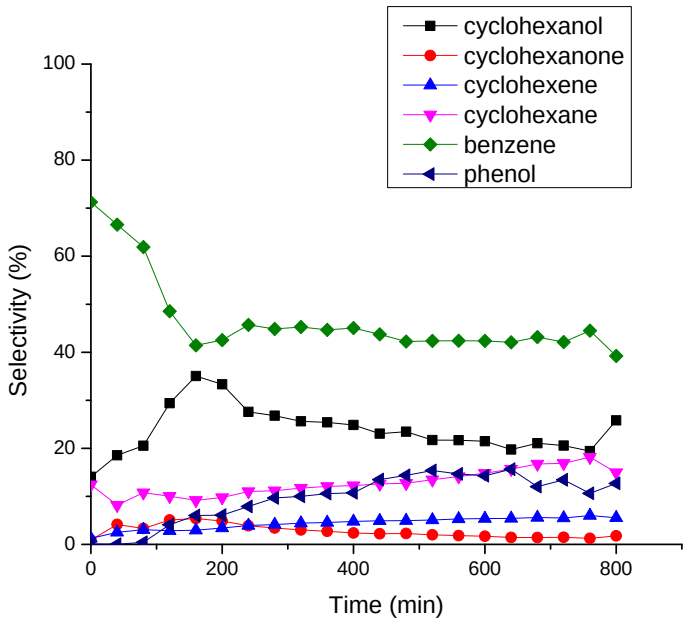

Figure 3.2.4.2 Product selectivities in diphenyl ether conversion at 300 ^{o}C, 100 psi with Ni-MCF catalyst (5 mg); H_2 flowrate 50 ml/min; WHSV 200 hr^{-1}

Figure 3.2.4.1 shows the conversion of diphenyl ether at WHSV of 200 hr^{-1} for 13 hours. The initial conversion was approximately 60%. The catalyst slowly deactivated in the first 3 hours; however, after 4 hours, the conversion decreased sharply to about 13% and stabilized at 10%.

Product selectivities for diphenyl ether conversion at WHSV of 200 hr^{-1} are shown in Figure 3.2.4.2. The two main products in the reaction were benzene and cyclohexanol, resulting from ether bond cleavage and saturation of one of the aromatic rings. Other products were phenol, which directly resulted from diphenyl ether bond cleavage, cyclohexene and cyclohexane, which were products from benzene hydrogenation and cyclohexanol dehydration. There was also less than 5% cyclohexanone in the products, which was an intermediate in the phenol hydrogenation to cyclohexanol reaction.

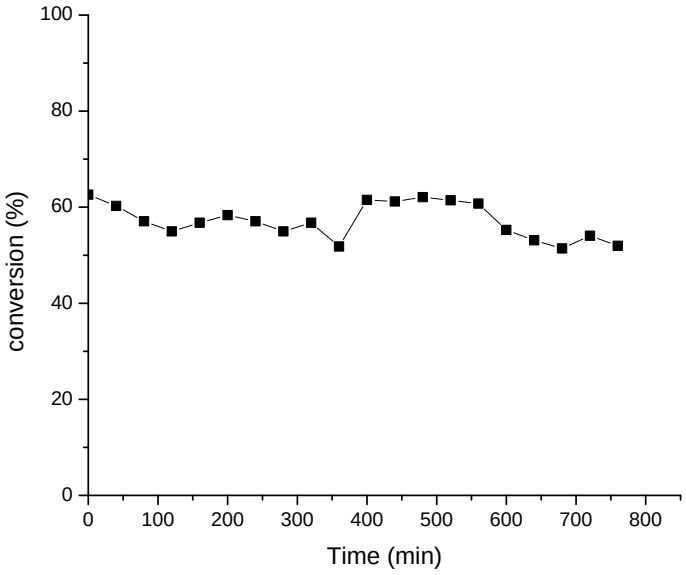

Figure 3.2.4.3 Diphenyl ether conversion at 300 ^{o}C, 100 psi with Ni-MCF catalyst (5 mg); H_2 flow rate 50 ml/min; WHSV 100 hr^{-1}

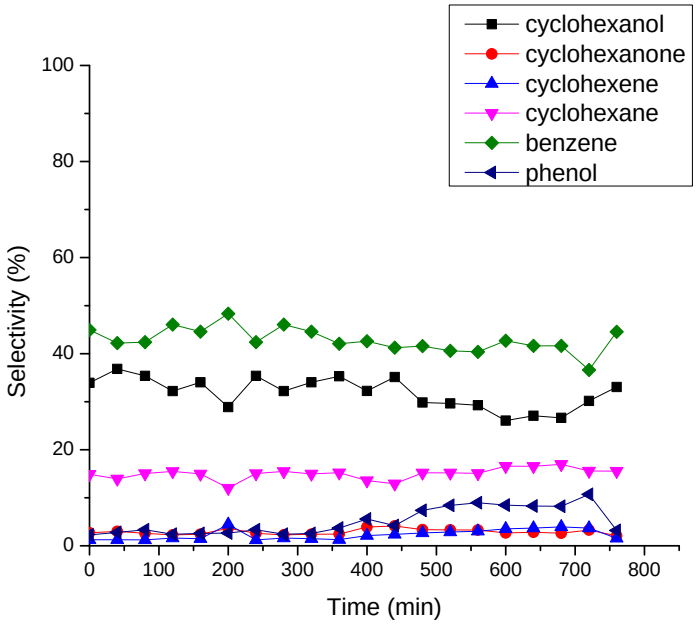

Figure 3.2.4.4 Product selectivities in diphenyl ether conversion at 300 ^{o}C, 100 psi with Ni-MCF catalyst (5 mg); H_2 flow rate 50 ml/min; WHSV 100 hr^{-1}

Figure 3.2.4.3 shows the conversion of diphenyl ether at WHSV of 100 hr^{-1}. At this WHSV the conversion was steady around 60% through the entire reaction time of 13 hours.

Products obtained with the diphenyl ether reaction at a WHSV of 100 hr^{-1} are shown in Figure 3.2.4.4: the major products are benzene, cyclohexanol, and other products are cyclohexane, cyclohexene, phenol and cyclohexanone. Since the conversion was stable throughout the reaction, selectivities of products did not change much, with that for benzene being 45% and that for cyclohexanol being 35%. Similar to the reaction at WHSV of 200 hr^{-1}, more benzene was produced than cyclohexanol.

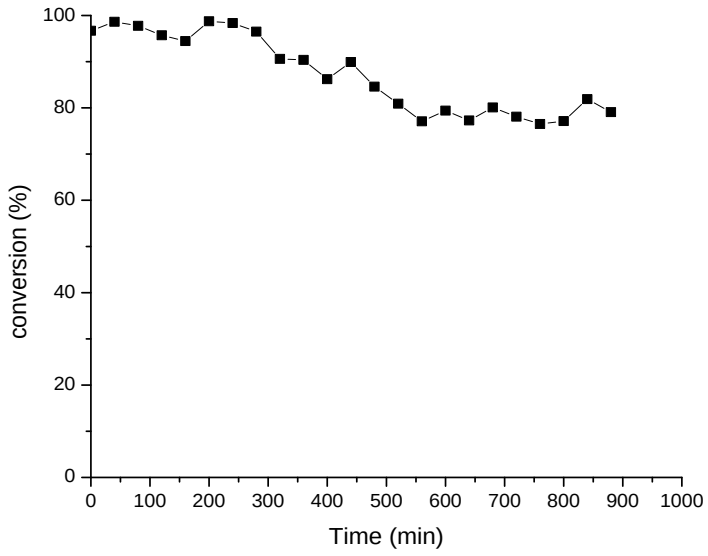

Figure 3.2.4.5 Diphenyl ether conversion at 300 ^{o}C, 100 psi with Ni-MCF catalyst (10 mg); H_2 flowrate 50 ml/min; WHSV 50 hr^{-1}

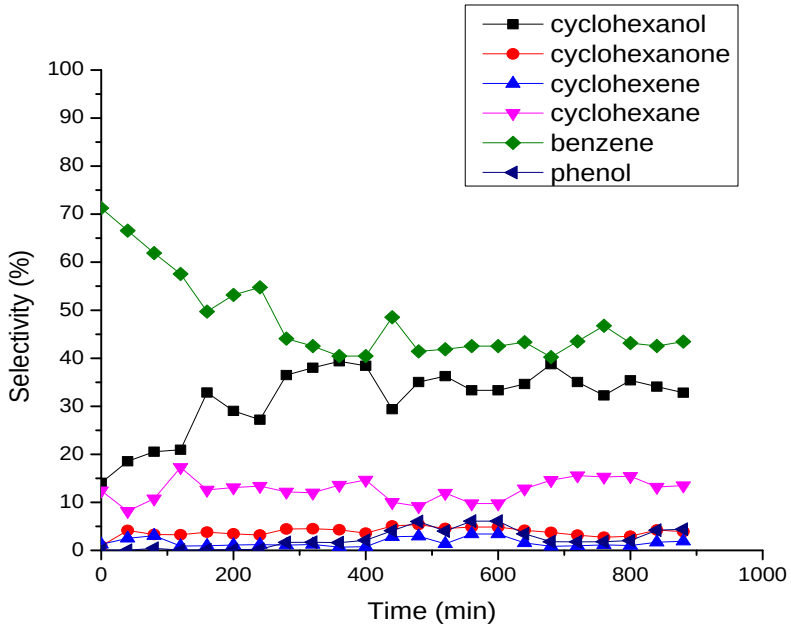

Figure 3.2.4.6 Product selectivities in diphenyl ether conversion at 300 ^{o}C, 100 psi with Ni-MCF catalyst (10 mg); H_2 flowrate 50 ml/min; WHSV 50 hr^{-1}

At a WHSV of 50 hr^{-1}, the conversion of diphenyl ether started at above 95%, which kept steady for more than 4 hours. Then the catalyst deactivated slowly, and conversion decreased to 75% and stabilized for 8 hours. Figure 3.2.4.6 shows products made in the reaction of diphenyl ether at WHSV of 50 hr^{-1}. Again, the main products were benzene and cyclohexanol, with the rest being cyclohexane, cyclohexene, cyclohexanone and phenol. Similar to the reaction at WHSV of 200 hr^{-1}, the selectivity for benzene decreased when reaching steady-state while that for cyclohexanol increased.

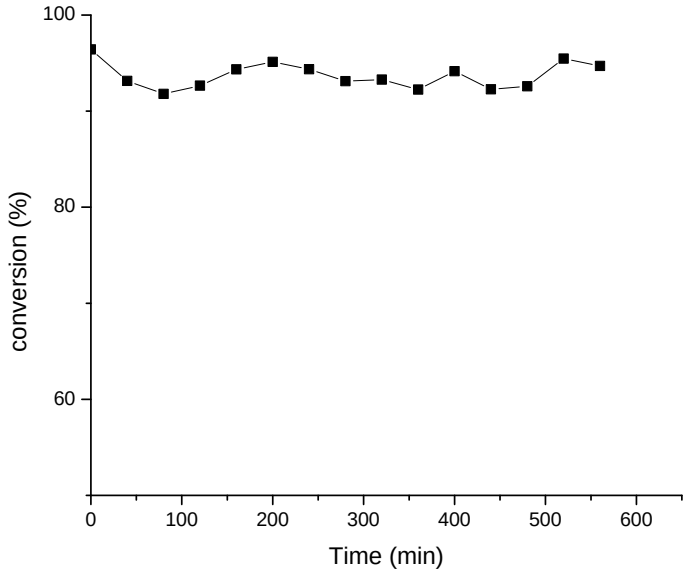

Figure 3.2.4.7 Diphenyl ether conversion at 300 ^{o}C, 100 psi with Ni-MCF catalyst (20 mg); H_2 flow rate 50 ml/min; WHSV 25 hr^{-1}

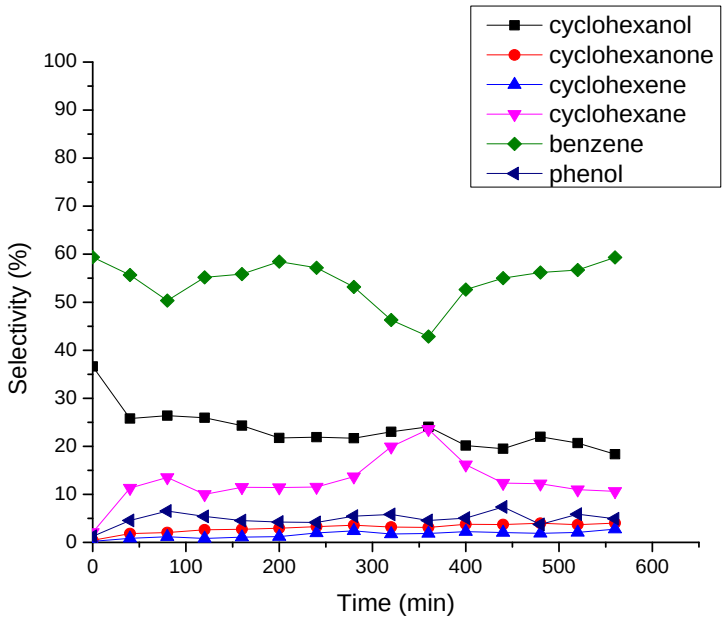

Figure 3.2.4.8 Product selectivities in diphenyl ether conversion at 300 ^{o}C, 100 psi with Ni-MCF catalyst (20 mg); H_2 flow rate 50 ml/min; WHSV 25 hr^{-1}

Figure 3.2.4.7 shows the conversion of diphenyl ether at a WHSV of 25 hr^{-1}. The conversion was around 95% for 10 hours. There was no obvious catalyst deactivation in this reaction. The products obtained in diphenyl ether reaction at WHSV of 25 hr^{-1} are shown in Figure 3.2.4.8. The selectivity to benzene was 60% and that to cyclohexanol was 25%. Other products were cyclohexane, phenol, cyclohexene, and cyclohexanone.

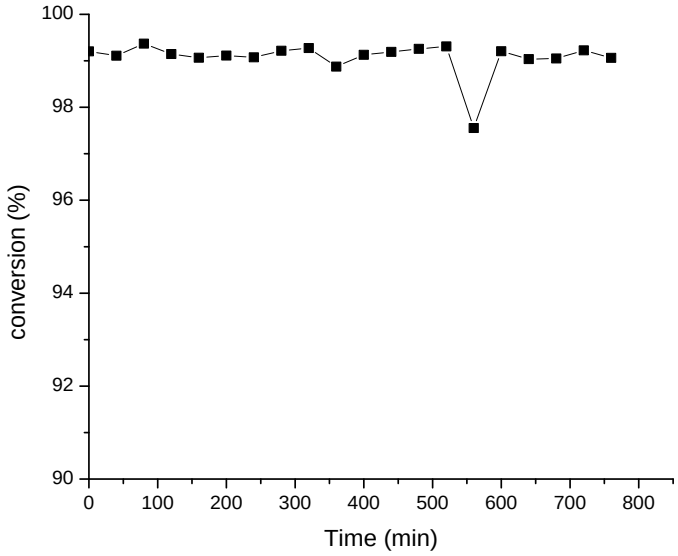

Figure 3.2.4.9 Diphenyl ether conversion at 300 ^{o}C, 100 psi with Ni-MCF catalyst (30 mg); H_2 flow rate 50 ml/min; WHSV 17 hr^{-1}

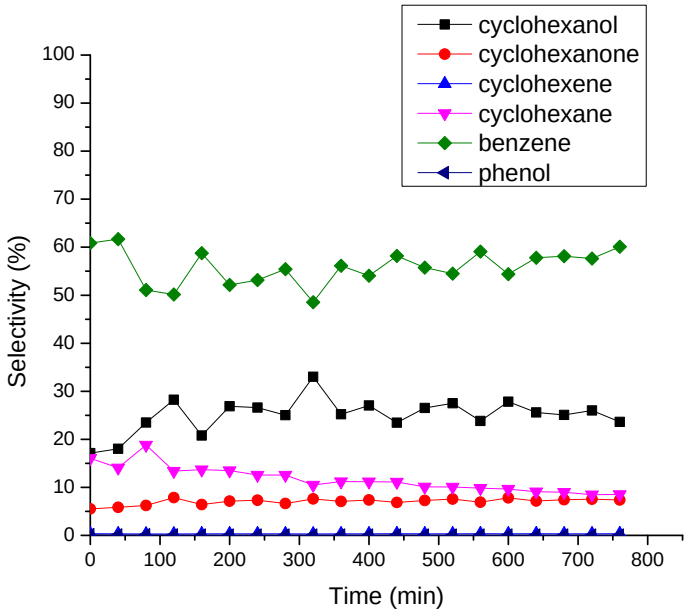

Figure 3.2.4.10 Product selectivities in diphenyl ether conversion at 300 ^{o}C, 100 psi with Ni-MCF catalyst (30 mg); H_2 flow rate 50 ml/min; WHSV 17 hr^{-1}.

Figure 3.2.4.9 shows the conversion of diphenyl ether at WHSV of 17 hr^{-1}. The conversion was steady around 99% for 14 hours, with no conversion drop due to catalyst deactivation.

The products obtained in the diphenyl ether reaction at WHSV of 17 hr^{-1} are shown in Figure 3.2.4.10. Similar to the reaction at WHSV of 25 hr^{-1}, 60% benzene and 25% cyclohexanol were obtained, with cyclohexane and cyclohexanone being minor products. At WHSV of 17 hr^{-1}, the phenol selectivity was below 1%, indicating that the number of catalytic sites was high enough to not only break diphenyl ether to monomeric products but also nearly fully hydrogenate the primary products.

Table 3.2.4.1 Summary of diphenyl ether conversions and product selectivitys. Reaction conditions: temperature 300 C; pressure, 100 PSI; H_2 flow rate, 50 mL/min; He flow rate, 50 mL/min; catalyst, Ni-MCF; WHSV, 17 hr^{-1}-200 hr^{-1}.

Diphenyl Ether				
WHSV hr^{-1}	Steady-state Major Products	Steady-state dipehnyl ether conversion %	Selectivity to cyclohexanol	Initial Major Products
200	Benzene; cyclohexanol	9	30	Benzene; cyclohexanol
100	Benzene; cyclohexanol	60	30	Benzene; cyclohexanol
50	Benzene; cyclohexanol	75	35	Benzene; cyclohexanol
25	Benzene; cyclohexanol;	94	25	Benzene; cyclohexanol
17	Benzene; cyclohexanol;	99	25	Benzene; cyclohexanol

For diphenyl ether, Ni-MCF shows great activity regarding ether bond breaking, which is in line with what other Ni-based catalysts have shown [99, 102, 103]. The experiments of diphenyl ether reacting with hydrogen from WHSV of 17 hr^{-1} to 200 hr^{-1} yielded mainly benzene and cyclohexanol. Other noticeable products were cyclohexane, which results from benzene ring saturation and cyclohexanol dehydration, and cyclohexanone, which is the intermediate from phenol conversion to cyclohexanol. The conversions through the entire runs of approximately 13 hours remained relatively stable for WHSV from 17 hr^{-1} to 100 hr^{-1}, unlike the obvious conversion decrease observed in the reactions of guaiacol and 4-methylguaiacol. This illustrates that the catalyst deactivation was much slower in the diphenyl ether reactions, which suggests less carbon deposition from diphenyl ether hydrogenation/hydrodeoxygenation products. This may be due to the lower oxygen content in the diphenyl ether reaction products than in the guaiacol and 4-methylguaiacol products. It is also possible that CO formed from methanol, a product in both guaiacol and 4-methylguaiacol hydrodeoxygenation, contributes to faster catalyst

deactivation in guaiacol and 4-methylguaiacol reactions by blocking active Ni sites. Table 3.2.4.1 summarizes the initial and steady-state products of diphenyl ether conversion at WHSV from 17 hr^{-1} to 200 hr^{-1}. The steady-state products, benzene and cyclohexanol, are the same ones as the initial products. Steady-state conversion increased as the WHSV decreased. The selectivity of cyclohexanol at all WHSV was lower than that of benzene. Scheme 3.2.4.1 shows the proposed reaction pathways of diphenyl ether hydrogenation based on the products obtained at a wide WHSV range. Benzene and phenol are produced from the ether bond cleavage, and then they can be hydrogenated to cyclohexane and cyclohexanone, and phenol could also be dehydrated to cyclohexane. Cyclohexanone can be further hydrogenated to cyclohexanol. The mass balance of reactions at all WHSVs closed within 95%. The ratio of the sum of benzene and cyclohexane to the sum of phenol and cyclohexanone and cyclohexanol is approximately 1.5:1, indicating that 1) the thermal decomposition rates of phenol, cyclohexanone and cyclohexanol are higher than those of benzene and cyclohexane due to the former ones having higher oxygen content [104, 105]. 2) There is a possibility that a fraction of cyclohexanol is dehydrated to cyclohexene and further hydrogenated to cyclohexane.

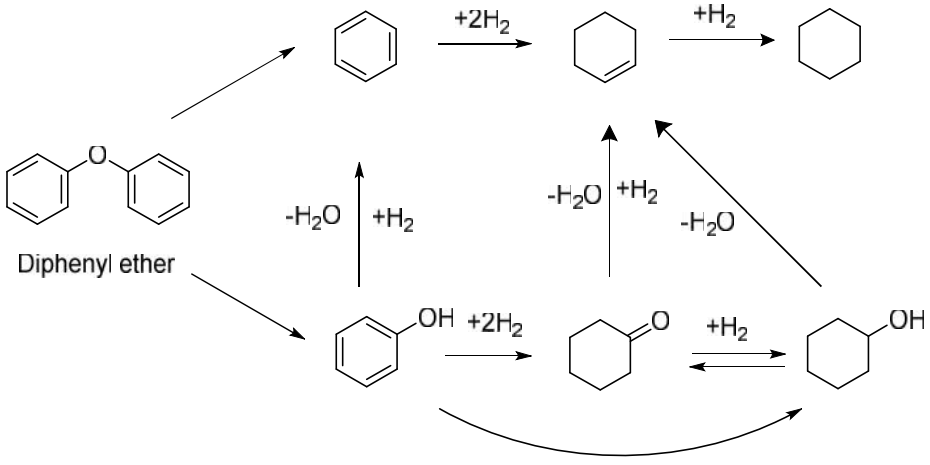

Scheme 3.2.4.1 Reaction pathways of diphenyl ether on Ni-MCF

3.2.5 The role of methanol in the conversion of diphenyl ether

Pseudo-first-order rate constants are determined by plotting ln(1/1-conversion) against 1/WHSV [81]: 1.69/hr for guaiacol, 3.00/hr for 4-methylguaiacol and 76.14/hr for diphenyl ether. The results show great differences in apparent reaction rate constants between the three, especially between guaiacol and diphenyl ether.

A hypothesis was considered that the deactivation rate difference was caused by the presence of methanol in products of guaiacol and 4-methylguaiacol reactions, which was not produced in diphenyl ether reactions. Methanol is believed to rapidly deactivate nickel based catalysts in transfer hydrogenation by attaching the methoxy group to active metal sites and blocking pores [106] and could play the same role in direct hydrogenation. CO formation from methanol could also contribute to catalyst deactivation. To examine this hypothesis, experiments were conducted by feeding diphenyl ether with 17 mol% (3 wt%) methanol into the reactor at WHSV of 50 hr^{-1} and comparing the resulting conversion with that from reaction without methanol in the feed to investigate the effect of methanol in catalyst deactivation.

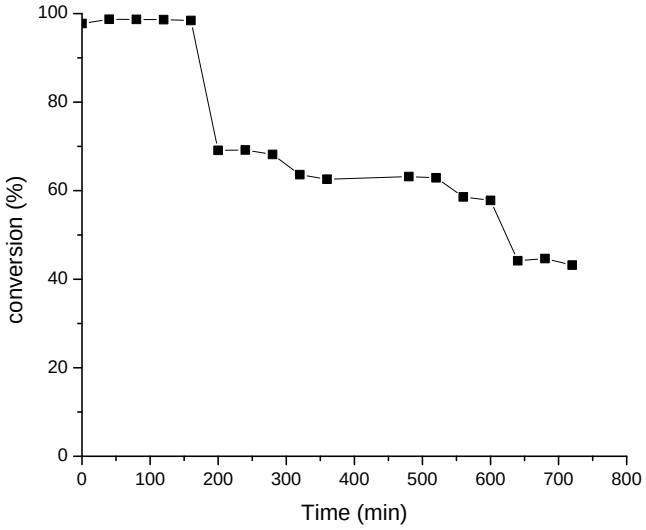

Figure 3.2.5.1 Diphenyl ether conversion at 300 ^{o}C, 100 psi with Ni-MCF catalyst (10 mg); H_2 flow rate 50 ml/min; WHSV 50 hr^{-}1; CH3OH content 17 mol%

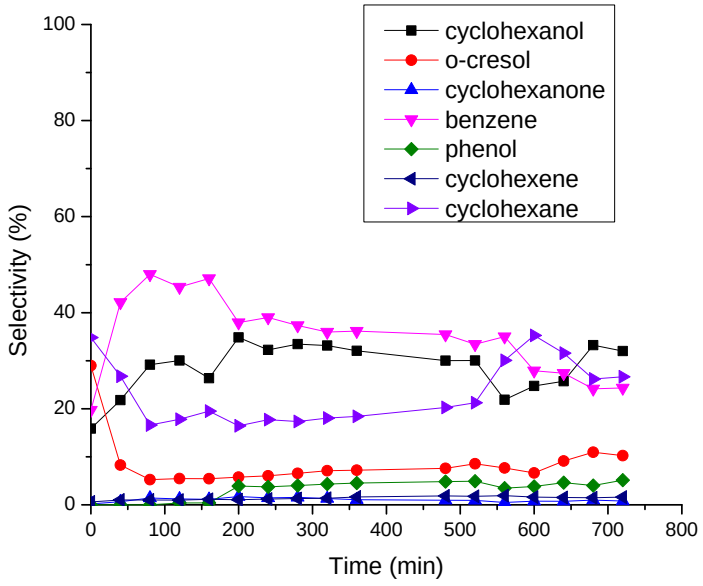

Figure 3.2.5.2 Product selectivities in diphenyl ether conversion at 300 ^{o}C, 100 psi with Ni-MCF catalyst (10 mg); H_2 flow rate 50 ml/min; WHSV 50 hr^{-}1; CH3OH content 17 mol%

At WHSV of 50 hr^{-1} with 17 mol% of methanol, the conversion of diphenyl ether started at above 95% and the high conversion kept for 4 hours, as in the reaction without

methanol in feed. The conversion then dropped to 70% in less than an hour and stayed at around 70% for another 4 hours before it decreased slightly again to its steady-state value of 55%. The steady-state conversion in the reaction with methanol in the feed was 55%, which is lower than the conversion (89%) of diphenyl ether without methanol at the same WHSV (50 hr^{-1})m which reveals that the presence of methanol did accelerate deactivation in the reaction, leading to faster catalyst deactivation.

In Figure 3.2.5.2 the product selectivities are shown. Major products were cyclohexanol, benzene, cyclohexane and *o*-cresol, the latter of which was not obtained in reactions of diphenyl ether without methanol at any WHSV. The selectivity of each major product was between 20% and 25%. The formation of *o*-cresol indicates changes in reaction pathways due to the reactivity of methanol. *o*-Cresol may result from the addition of a methyl group from methanol to phenol, which is an acid catalyzed reaction. The acidity could be provided by the SiO_2 support in catalyst.

Reaction pathways summary

Scheme 3.2.5.1 summaries all the probable reaction pathways of guaiacol, 4-methylguaiacol and diphenyl ether over Ni-MCF. It can be seen that guaiacol firstly underwent demethoxylation to phenol and hydrogenation to 2-methoxyclohexanol and 2-methoxycyclohexanone whereas 4-methylguaiacol was demethoxylyzed to p-cresol and hydrogenolyzed to 4-methylcatechol. This indicates that with the compound with an extra methyl group 4-methylguaiacol is more reluctant to aromatic ring hydrogenation. A possible explanation is that intermediate 2-methoxycyclohexa-2,5-dienone was formed during the hydrogenation of guaiacol, but in 4-methylguaiacol hydrogenation, the

formation of 2-methoxy-4-methylcyclohexa-2,5-dienone was less favorable due to the repulsion between the carbonanion and electron-rich methyl group (Scheme 3.2.5.2). Thus 4-methylguaiacol was hydrogenolyzed to 4-methylcatechol and *p*-cresol before aromatic ring hydrogenation. Diphenyl ether underwent ether bond cleavage before hydrogenation of the aromatic rings. Products phenol and benzene were further hydrogenated. In 4-methyguaiacol and diphenyl ether conversions, small fraction of fully hydrogenated products methylcyclohexane and cyclohexane were obtained from 4-methylcyclohexanol and cyclohexanol dehydration, showing acidity in the catalyst support.

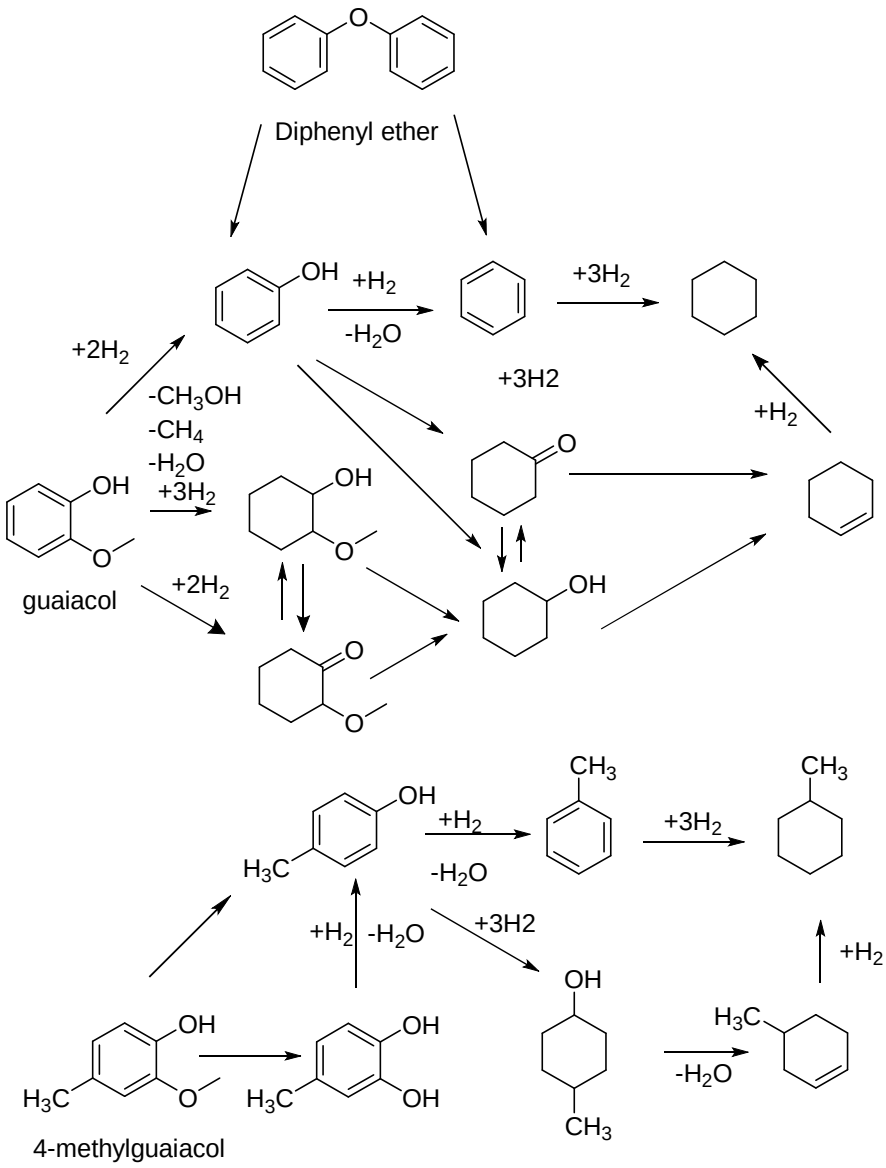

Scheme 3.2.5.1 Pathways of guaiacol, 4-methylguaiacol and diphenyl ether over Ni-MCF

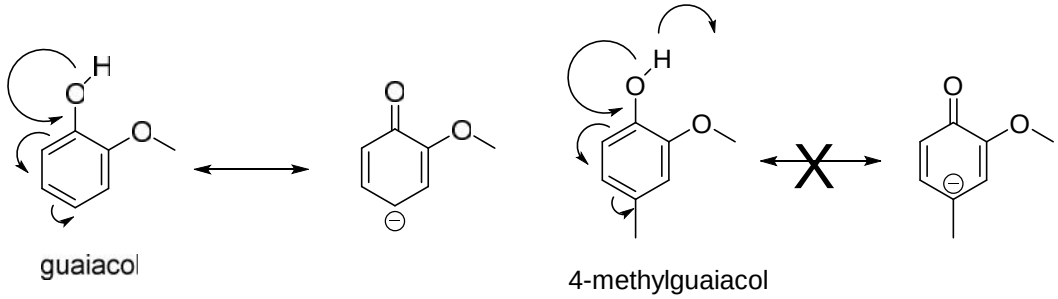

Scheme 3.2.5.2 Differences in guaiacol and 4-methylguaiacol reaction pathways

3.3 Spent catalyst characterization

To examine the factors that contributed to catalyst deactivation, which caused significant decreases in the reaction conversion, the catalysts after reactions were collected and characterized using N_2 physisorption, XAS, XRD and TGA to reveal structural changes before and after reactions.

3.3.1 Nitrogen Physisorption

Nitrogen physisorption was conducted on the used catalysts to illustrate the structural changes of the catalyst caused by both coke formation and silica support deformation.

Table 3.3.1.1 Nitrogen physisorption results of fresh, reduced and spent Ni-MCF

	BET surface area (m^2/g)	BdB-FHH Pore volume (cm^3/g)
Before reduction	418	1.52
After reduction & Before reaction	340	1.07
After Guaiacol reactions	205	0.60
After 4-Methylguaiacol reactions	262	0.86
After Diphenyl ether reactions	334	0.94

Table 3.3.1.1 lists the BET surface areas and BdB-FHH pore volumes of the fresh catalyst (calcined catalyst), reduced catalyst and spent catalyst after guaiacol, 4-methylguaiacol and diphenyl ether reactions. Both of the surface area and pore volume decreased after catalyst reduction. The surface area of the reduced catalyst decreased by 18% and the pore volume decreased by 29% compared with the fresh catalyst. This indicates that the silica support structure was transformed during the high temperature reduction and some porosity was lost. The order of magnitude of both the surface area

and pore volume of the spent catalyst after reaction is diphenyl ether > 4-methylguaiacol > guaiacol. This order suggests that pore blockage was most serious after guaiacol reactions, suggesting most coke formation happened in the guaiacol reaction among the three. This observation can explain why guaiacol conversion decreased more rapidly than 4-methylguaiacol, and 4-methylguaiacol conversion decreased faster than diphenyl ether.

3.3.2 X-ray absorption spectroscopy

To understand the change in oxidation state of the metal particles in the catalyst, X-ray absorption spectroscopy was performed on the spent Ni-MCF after 4-methylguaiacol reactions.

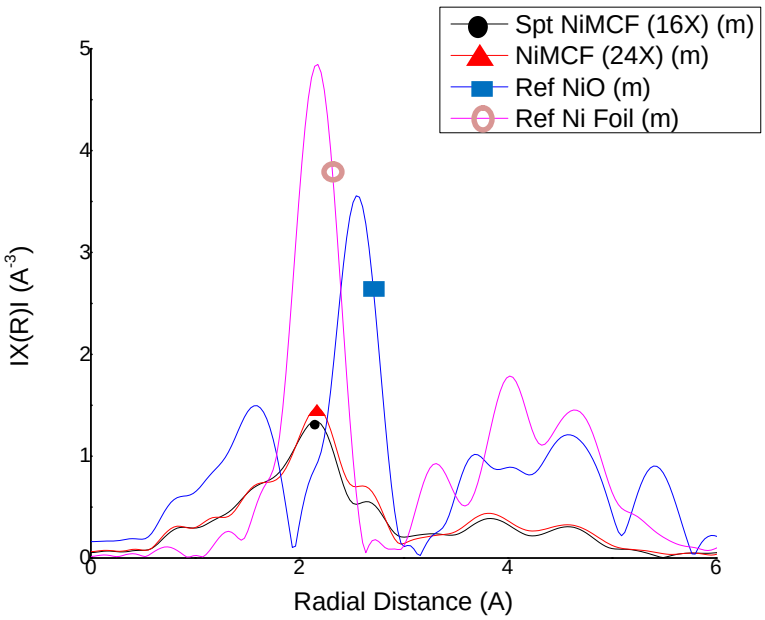

Figure 3.3.2.1 Extended X-Ray absorption fine structure of reduced and spent Ni-MCF (4-methylguaiacol) with NiO and Ni foil references

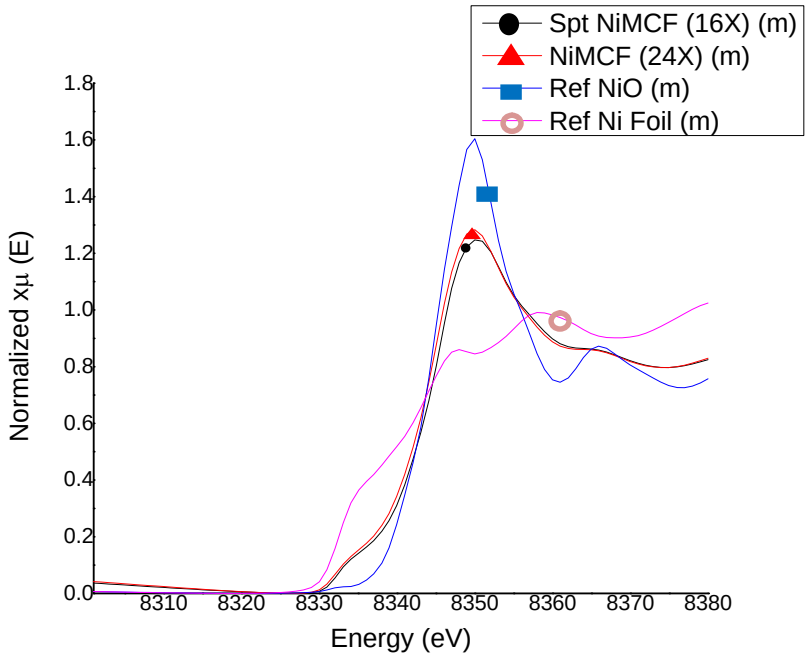

Figure 3.3.2.2 X-ray absorption near edge structure of reduced and spent Ni-MCF (4-methylguaiacol) with NiO and Ni foil references.

Both EXAFS and XANES results show no significant change in the average oxidation state of Ni in the spent Ni-MCF or in the local Ni bonding compared with the non-reacted Ni-MCF. The spent catalyst still had Ni-Ni and Ni-O bond character after reactions, and there was no noticeable difference in the intensity of the Ni-Ni and Ni-O signals before and after reaction. Since the spent catalyst did not undergo passivation after the reaction before removal from the reactor, there could be larger amount of Ni-Ni in the spent catalyst than in the unreacted one due to additional reduction under reaction conditions. If this occurs, the additional Ni(0) species were likely to oxidize upon removal from the reactor.

3.3.3 X-ray diffraction

Along with XAS analysis, XRD was also done to elucidate the changes in nickel/nickel oxide phases in the catalyst after reaction. XRD patterns of the spent catalysts after guaiacol, 4-methylguaiacol and diphenyl ether reactions are shown in Figure 3.3.3.1 – 3.3.3.3. A significant change of the crystallinity was not observed in the catalyst used in guaiacol hydrogenation, although there was an additional peak that represents additional Ni metal (Ni (200)) in addition to the Ni (111), which suggests larger reduced metal domains.

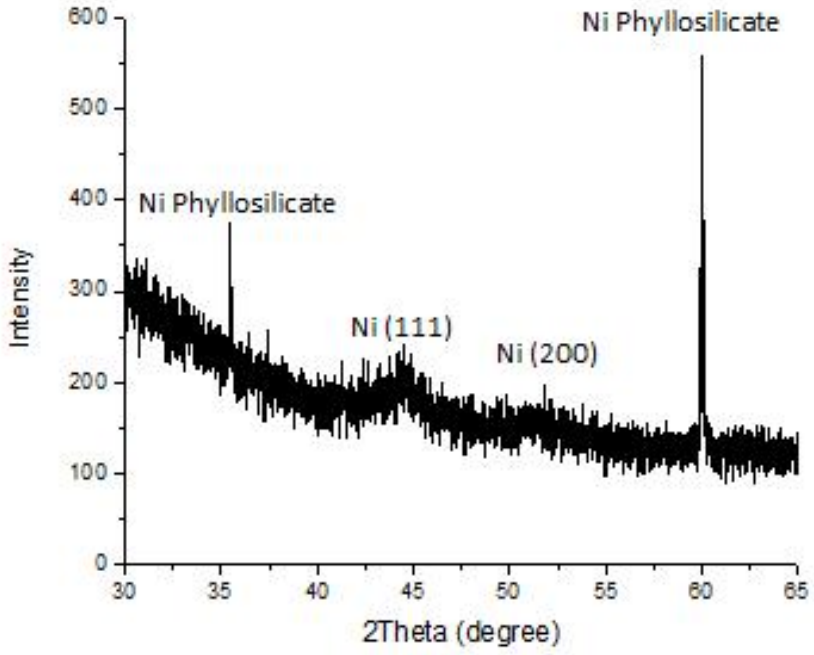

Figure 3.3.3.1 XRD pattern of spent Ni-MCF after guaiacol reactions at WHSV of 10 hr^{-1}

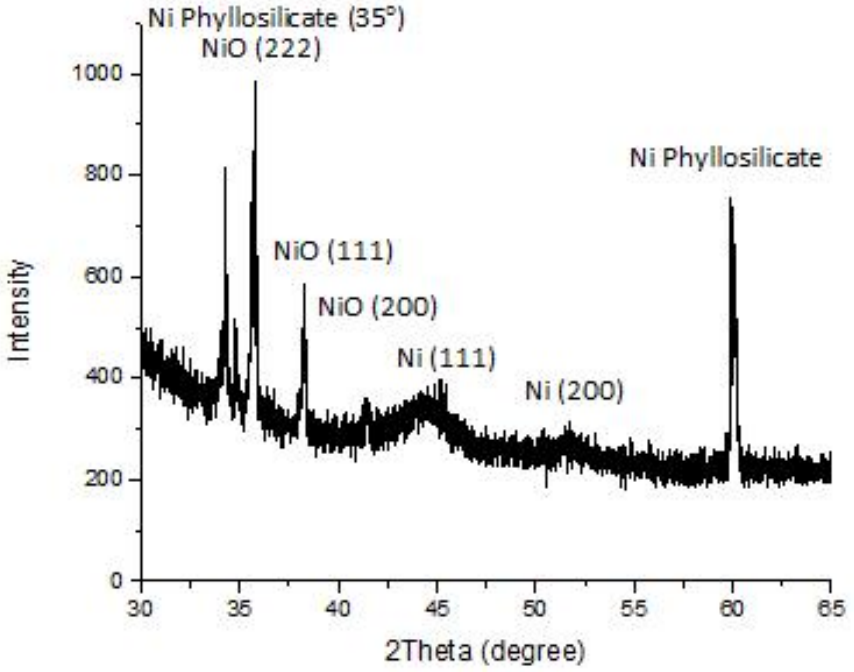

Figure 3.3.3.2 XRD pattern of spent Ni-MCF after 4-methylguaiacol reactions at WHSV of 10 hr^{-1}

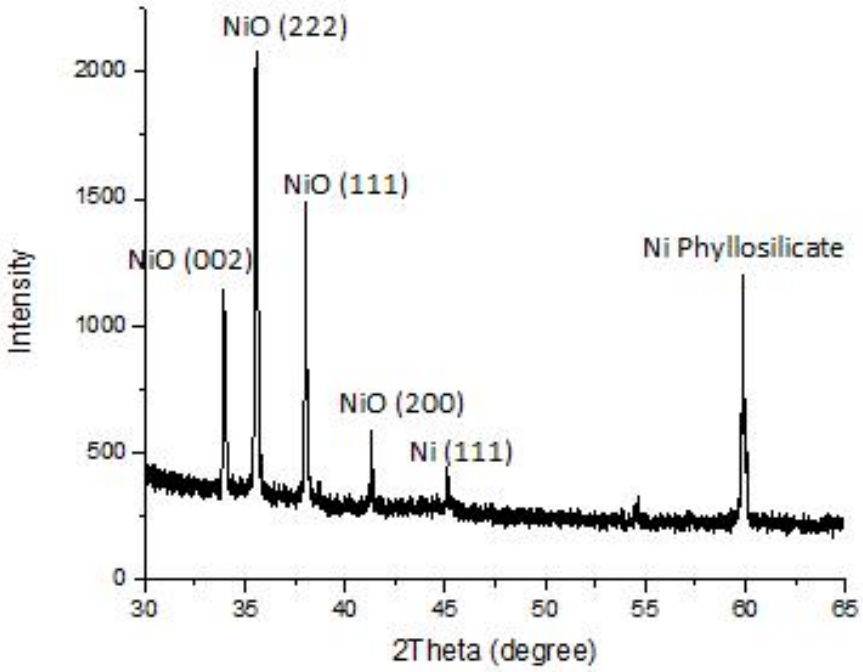

Figure 3.3.3.3 XRD pattern of spent Ni-MCF after diphenyl ether reactions at WHSV of 10 hr^{-1}

On the other hand, the XRD patterns of the spent catalyst after 4-methylguaiacol and diphenyl ether reactions show more obvious changes in the crystalline phases. Both patterns indicate that the sample is more crystalline overall, with many different strong peaks associated with NiO and Ni phyllosilicate domains after reactions. The restructuring of the sample under reaction conditions producing enhanced NiO crystallinity after reactions may be due to exposure to high temperature water formed during reactions [14]. The increase in Ni phyllosilicate domain suggests increase in the interactions of Ni/NiO with silica support during reactions to form more Ni silicate. The sharper shape of the peaks after reactions indicates that the crystalline NiO and Ni domains are larger, which may be due to the formation of clusters of NiO and Ni during the collapse of the thin-walled silica support.

3.3.4 Thermogravimetric analysis

Thermogravimetric analysis was used to identify the extent of coke formation on the catalyst. The thermogravimetric analysis (TGA) results for spent Ni-MCF after guaiacol, 4-methylguaiacol, diphenyl ether and diphenyl ether with 17 mol% methanol reactions are listed in Table 3.3.4.1.

Table 3.3.4.1 TGA results of spent Ni-MCF

Ni-MCF	% Wt. Low Temperature (200C to 420C) Coke	% Wt. High Temperature (420C to 600C) Coke	Low Temperature weight loss/Catalyst weight	high Temperature weight loss/Catalyst weight
After reaction of Guaiacol	3.1	7.0	0.04	0.08
After reaction of 4-Methylguaiacol	4.5	5.4	0.05	0.06
After reaction of diphenyl ether	6.0	2.8	0.07	0.03
After reaction of diphenyl ether with MeOH	5.1	3.2	0.06	0.04

By comparing the low temperature (200 °C to 420 °C) coke weight/catalyst weight and high temperature (420 °C to 600 °C) coke weight/catalyst weight among the four samples, it is clear that the highest amount of low temperature coke was formed on the catalyst in diphenyl ether reactions and the highest amount of high temperature coke was formed on the catalyst in guaiacol reactions. The order of high temperature coke formation/catalyst weight is guaiacol > 4-methylguaiacol > diphenyl ether with 17 mol% methanol > diphenyl ether. According to the results from the reaction studies, the order of the conversions of reactants at the same WHSV is diphenyl ether > diphenyl ether with 17 mol% methanol > 4-methylguaiacol > guaiacol. These results indicate that higher amount of high temperature coke formation led to more catalyst site/pore blockage, showing correlation between reactivity and residual carbon species on the catalyst.

By comparing the N_2 physisorption, XAS and XRD results of catalyst before and after reactions, it can be summarized that Ni-MCF underwent both silica support structure and Ni crystal structure changes during the reactions of guaiacol, 4-methylguaiacol and diphenyl ether. Carbonaceous species deposited on the catalyst during reaction, which

caused catalyst deactivation as the reaction proceeded. Deformation of the silica support structure (reflected by loss of surface area) due to steaming from the water formed during reduction and reaction might cause clustering of Ni, making it less well-dispersed, lowering the accessibility of reactants to catalytic sites and thus decreased reaction conversion.

CHAPTER 4

CONCLUSIONS AND FUTURE WORK RECOMMENDATIONS

The study has focused on the use of hydrothermally synthesized Ni-MCF in the hydrodeoxygenation/hydrogenation of guaiacol, 4-methylguaiacol and diphenyl ether. Characterizations such as TPR, XRD and TEM suggest the incorporation of Ni into the silica support to form Ni silicate, making it difficult to reduce to Ni^0. EXAFS of reduced and passivated Ni-MCF showed that NiO formed through hydrothermal synthesis and was partially reduced to Ni during reduction. Ni-MCF successfully converted guaiacol, 4-methylguaiacol and diphenyl ether to monocyclic products. Guaiacol conversion decreased quickly as the reaction proceeded, suggesting fast catalyst deactivation. In the meantime, the selectivities to cyclohexanol and cyclohexanone in the guaiacol reaction were both below 1% at steady-state for all WHSVs tested. Instead, 2-methoxycyclohexanol and 2-methoxycyclohexanone were dominant steady-state products, suggesting the lack of hydrogenolysis ability of catalyst once deactivated. On the other hand, direct hydrogenation of 4-methylguaiacol was not favored. 4-methylguaiacol produced mainly *p*-cresol and methyl-substituted cyclohexanol hydrogenated from *p*-cresol at steady-state. Among the three reactants, diphenyl ether achieved the best selectivities to the desired products, cyclohexanol and cyclohexanone, and maintained high conversion at relatively high WHSVs, which may be attributed to the lack of methoxy group in diphenyl ether. In the hydrogenation of diphenyl ether with methanol in the feed, acceleration of catalyst deactivation was shown. Characterizations (EXAFS and XRD) of spent catalyst confirmed the presence of Ni(0) in the catalyst during reactions. TGA results confirmed coke formation on the catalyst after guaiacol, 4-

methylguaiacol and diphenyl ether reactions. These carbonaceous species caused catalyst deactivation by depositing on the catalyst during reaction. The order of high temperature coke formation/catalyst weight is guaiacol > 4-methylguaiacol > diphenyl ether with 17 mol% methanol > diphenyl ether. This result is in compliance with the N_2 physisorption results, where the spent catalyst surface area after guaiacol reactions was the lowest and after diphenyl ether reaction the highest, suggesting the most serious pore blocking happened in guaiacol reactions. It also explains why the order of the conversions of reactants at the same WHSV was diphenyl ether > 4-methylguaiacol > guaiacol. Guaiacol conversion decreased the fastest because of heavy coke formation on the catalyst.

Future work recommendations

In this study only three models of lignin fragments were investigated. The future could be focused on more complex lignin/bio-oil model compounds and their mixtures or even actual lignin/bio-oil. To achieve better conversion and higher selectivity of desired products, catalyst configuration, including metal loading and dispersion, or the support material could be tuned to limit decomposition of products and reactants, which causes coke formation. By varying WHSV in reactions, it seems that an optimization of catalyst loading in maintaining conversion at desired level for a specific period of time could be achieved. This may be of interest in the commercialization of this process where the balance of catalyst usage and conversion needs to be developed. Except for the diphenyl ether reaction at WHSV of 50 hr^{-1}, the reaction time-on-stream never exceeded 13 hours. It is worthwhile to do longer time-on-stream reactions since it sheds a light on the extent of the stability of catalyst at different WHSVs. Recycling of the catalyst was not

performed in this study, which could be an important extension for commercialization of the hydrogenation process. Taking factors such as catalyst production price, catalyst deactivation, reaction conversion, target products selectivity and catalyst recyclability into account, a price comparison could be made on the cyclohexanol produced by lignin waste with that produced by petroleum to determine the feasibility of using lignin waste as a renewable Nylon 6 production source.

REFERENCES

1. Smalley Institute Grand Challenges. 2008 [cited 2011 Feb. 4].

2. Key World Energy Statistics. 2012, International Energy Agency: Paris, France.

3. Owen, N.A., O.R. Inderwildi, and D.A. King, The status of conventional world oil reserves-Hype or cause for concern? Energy Policy, 2010. 38(8): p. 4743-4749.

4. Technology roadmap-Biofuels for transport, IEA

5. EPA Finalizes Regulations for the National Renewable Fuel Standard Program for 2010 and Beyond, O.o.T.a.A. Quality, Editor. 2010, US EPA.

6. Hubbert, M.K., Energy from Fossil Fuels. Science, 1949. 109: p. 103-109.

7. Hubbert, M.K., Nuclear Energy and the Fossil Fuels. 1956, Shell Development Company - Exploration and Poduction Research Division.

8. Annual Energy Review 2011, U. EIA, Editor. 2012.

9. Montgomery, Carl T.; Smith, Michael B. (2010-12-105). Hydraulic fracturing. History of an enduring technology". JPT Online (Society of Petroleum Engineers): 26–41.

10. Crude Oil: Uncertainty about Future Oil Supply Makes It Important to Develop a Strategy for Addressing a Peak and Decline in Oil Production, U.G.A Office, Editor. 2007: Washington, D.C.

11. Bowyer, J., R. Shmulsky, and J. Haygreen, Forest Products and Wood Science: An Introduction. 5th ed. 2007, Oxford, UK: Blackwell Publishing.

12. Perlack, R., et al., Biomass as Feedstock for a Bioenergy and Bioproducts Industry: The Technical Feasibility of a Billion- Ton Annual Supply. 2005, Oak

Ridge National Laboratory, US Department of Agriculture, US Department of Engergy: Oak Ridge, TN.

13. Fargione, J.E., R.J. Plevin, and J.D. Hill, The Ecological Impact of Biofuels. Annual Review of Ecology, Evolution, and Systematics, 2010. 41(1): p. 351-377.

14. Ragauskas, A.J., et al., The path forward for biofuels and biomaterials. Science, 2006. 311(5760): p. 484-489.

15. Sims, R., et al., From 1st- to 2nd- Generation Biofuel Technologies: An overview of current industry and R&D activities. 2008, International Enery Agency: Paris, France.

16. World Energy Outlook 2010 Executive Summary. 2010, International Energy Agency: Paris, France.

17. http://www.umsl.edu/services/ora/News%20and%20Events/wang-biofuels.html

18. Transport, Energy and CO2: Moving Towards Sustainability. 2009, International Energy Agency: Paris, France.

19. Demirbas, M.F., Biorefineries for biofuel upgrading: A critical review. Applied Energy, 2009. 86: p. S151-S161.

20. Huber, G.W. and J.A. Dumesic, An overview of aqueous-phase catalytic processes for production of hydrogen and alkanes in a biorefinery. Catalysis Today, 2006. 111(1-2): p. 119-132.

21. Top Value Added Chemicals from Biomass: Volume I - Results of Screening for Potential Candidates from Sugars and Synthesis Gas, T. Werpy and G. Petersen, Editors. 2004, Pacific Northwest National Laboratory (PNNL) National Renewable Energy Laboratory (NREL).

22. Stocker S (2008) Angew Chem Int Ed Engl 47: 9200

23. Milne T, Agblevor F, Davis M, Deutch S, Johnson D (1997) In: Bridgewater AV, Boocock DGB (eds) Developments in Thermal Biomass Conversion. Blackie, London

24. Kamm, B., et al., Lignocellulose-based Chemical Products and Product Family Trees, in Biorefineries - Industrial Processes and Products, B. Kamm, P.R. Gruber, and M. Kamm, Editors. 2006, Wiley-VCH Verlag GmbH & Co. KGaA: Weinheim.

25. Guerra, A., et al., Comparative evaluation of three lignin isolation protocols for various wood species. Journal of Agricultural and Food Chemistry, 2006. 54(26): p. 9696-9705.

26. Guerra, A., et al., Toward a better understanding of the lignin isolation process from wood. Journal of Agricultural and Food Chemistry, 2006. 54(16): p. 5939-5947.

27. Boerjan, W., J. Ralph, and M. Baucher, Lignin biosynthesis. Annual Review of Plant Biology, 2003. 54: p. 519-546.

28. Ralph, J., et al., Lignins: Natural polymers from oxidative coupling of 4-hydroxyphenylpropanoids. Phytochemistry Reviews, 2004. 3(1-2): p. 29-60.

29. Meister, J.J., Modification of lignin. Journal of Macromolecular Science-Polymer Reviews, 2002. C42(2): p. 235-289.

30. Hon, D. and N. Shiraishi, Wood and Cellulosic Chemistry. 2000, New York: Marcell and Decker.

31. Lin, L. and C. Dence, eds. Methods in Lignin Chemistry. 1992, Springer-Verlag: New York.

32. S. Yaman, Energy Conversion and Management 45 (5) (2004) 651–671.

33. A. Bridgwater, Biomass and Bioenergy (2011), http://dx.doi.org/10.1016/j.biombioe.2011.01.048.

34. D. Bulushev, J. Ross, Catalysis Today 171 (1) (2011) 1–13.

35. M.F. Demirbas, M.F. Balat M., Journal of Scientific and Industrial Research 66 (2007) 797–804.

36. R. N. Olcese et al. Hydrodeoxygenation of guaiacol, a surrogate of lignin pyrolysis vapors, over iron based catalysts: kinetics and modeling of the lignin to aromatics integrated process, Energy & Fuels

37. Q. Lu, W. –Z. Li, X.-F. Zhu, Energy Convers. Manag. 50 (2009) 1376-1383

38. K. L. Deutsch and B. H. Shanks, Hydrodeoxygenation of Lignin Model Compounds over a Copper Chromite Catalyst, Applied Catalysis A: General 447-448

39. E. Laurent, B. Delmon, Appl. Catal. A 109 (1994) 97–115.

40. M. Ferrari, R. Maggi, B. Delmon, P. Grange, J. Catal. 198 (2001) 47–55.

41. M. D. Guillen et al. GC/MS analysis of lignin monomers, dimers and trimers in liquid smoke flavorings, J Sci Food Agric 79: 1889-1903 (1999)

42. I.T.Ghampson,C.Sepulveda,R.Garcia,B.G.Frederick,M.C.Wheeler,N.Escalona, W.J. DeSisto, Appl. Catal. A 413–414 (2012) 78–84.

43. A.L. Jongerius, R. Jastrzebski, P.C.A. Bruijnincx, B.M. Weckhuysen, J. Catal. 285 (2012) 315–323.

44. C.V. Loricera, B. Pawelec, A. Infantes-Molina, M.C. Alvarez-Galvan, R. Huirache-Acuna, R. Nava, J.L.G. Fierro, Catal. Today 172 (2011) 103–110.

45. M. Badawi, J.F. Paul, S. Cristol, E. Payen, Catal. Commun. 12 (2011) 901–905.

46. Y. Romero, F. Richard, S. Brunet, Appl. Catal. B: Environ. 98 (2010) 213–223.

47. A. Pinheiro, D. Hudebine, N. Dupassieux, C. Geantet, Energy Fuels 23 (2009) 1007–1014.

48. O.I. Senol, E.M. Ryymin, T.R. Viljava, A.O.I. Krause, J. Mol. Catal. A: Chem. 277 (2007) 107–112.

49. T.R. Viljava, E.R.M. Saari, A.O.I. Krause, Appl. Catal. A: Gen. 209 (2001) 33–43.

50. T.R. Viljava, R.S. Komulainen, A.O.I. Krause, Catal. Today 60 (2000) 83–92.

51. A. Centeno, E. Laurent, B. Delmon, J. Catal. 154 (1995) 288–298.

52. E. Laurent, B. Delmon, Appl. Catal. A: Gen. 109 (1994) 77–96.

53. E. Laurent, B. Delmon, J. Catal. 146 (1994) 281–291.

54. E. Laurent, B. Delmon, Appl. Catal. A: Gen. 109 (1994) 97–115.

55. S.B. Gevert, M. Eriksson, P. Eriksson, F.E. Massoth, Appl. Catal. A: Gen. 117 (1994) 151–162.

56. E. Laurent, B. Delmon, Ind. Eng. Chem. Res. 32 (1993) 2516–2524.

57. J.B.S. Bredenberg, M. Huuska, J. Raty, M. Korpio, J. Catal. 77 (1982) 242–247.

58. H. Weigold, Fuel 61 (1982) 1021–1026.

59. S.J. Hurff, M.T. Klein, Ind. Eng. Chem. Fundam. 22 (1983) 426–430.

60. E.O. Odebunmi, D.F. Ollis, J. Catal. 80 (1983) 56–64.

61. R.K.M.R. Kallury, T.T. Tidwell, D.G.B. Boocock, D.H.L. Chow, Can. J. Chem. 62 (1984) 2540–2545.

62. M. Huuska, J. Rintala, J. Catal. 94 (1985) 230–238.

63. R.K.M.R. Kallury, W.M. Restivo, T.T. Tidwell, D.G.B. Boocock, A. Crimi, J. Douglas, J. Catal. 96 (1985) 535–543.

64. F.P. Petrocelli, M.T. Klein, Ind. Eng. Chem. Prod. Res. Dev. 24 (1985) 635–641.

65. B.S. Gevert, J.E. Otterstedt, F.E. Massoth, Appl. Catal. 31 (1987) 119–131.

66. J.B. Bredenberg, M. Huuska, P. Toropainen, J. Catal. 120 (1989) 401–408.

67. P. Toropainen, J.B. Bredenberg, Appl. Catal. 52 (1989) 57–68.

68. V.A. Yakovlev, S.A. Khromova, O.V. Sherstyuk, V.O. Dundich, D.Y. Ermakov, V.M. Novopashina, M.Y. Lebedev, O. Bulavchenko, V.N. Parmon, Catal. Today 144 (2009) 362–366.

69. A. Popov, E. Kondratieva, J.M. Goupil, L. Mariey, P. Bazin, J.P. Gilson, A. Travert, F. Mauge, J. Phys. Chem. C 114 (2010) 15661–15670.

70. C.R. Lee, J.S. Yoon, Y.W. Suh, J.W. Choi, J.M. Ha, D.J. Suh, Y.K. Park, Catal. Commun. 17 (2012) 54–58.

71. G.M. Dolce, P.E. Savage, L.T. Thompson, Energy Fuels 11 (1997) 668–675.

72. M. Nagai, Y. Goto, A. Irisawa, S. Omi, J. Catal. 191 (2000) 128–137.

73. J. Monnier, H. Sulimma, A. Dalai, G. Caravaggio, Appl. Catal. A 382 (2010) 176–180.

74. I.T.Ghampson,C.Sepulveda,R.Garcia,B.G.Frederick,M.C.Wheeler,N.Escalona, W.J. DeSisto, Appl. Catal. A 413–414 (2012) 78–84.

75. M. V. Bykova et al. Guaiacol hydrodeoxygenation kinetics with catalyst deactivation taken into consideration, Kinetivs and Catalysis, 2013, Vol 54, No. 1, pp. 40-48

76. M. V. Bykova et al. Ni-based catalysts as promising systems for crude bio-oil upgrading:guaiacol hydrodeoxygenation study, Applied Catalysis B: Environmental 113-114 (2012) 296-307

77. K. L. Deutsch and B. H. Shanks, Hydrodeoxygenation of Lignin Model Compounds over a Copper Chromite Catalyst, Applied Catalysis A: General 447-448 (2012) 144-150

78. Y. Lin et al. Catalytic hydrodeoxygenation of guaiacol on Rh-based and sulfided CoMo and NiMo catalysts, Energy Fuels 2011, 25, 890-896

79. A. Gutierrez et al. Hydrodeoxygenation of guaiacol on noble metal catalysts, Catalysis Today 147 (2009) 239-246

80. C. Zhao et al. Aqueous-phase hydrodeoxygenation of bio-derived phenols to cycloalkanes, Journal of Catalysis 280 (2011) 8-16

81. Eun-Jae Shin and Mark A. Keane, Gas-phase hydrogenation/hydrogenolysis of phenol over supported Ni catalysts, Ind. Eng. Chem. Res. 2000, 39, 883-892

82. M. V. Olarte, Base-catalyzed depolumerization of lignin and hydrodeoxygenation of ligin model compounds for alternative fuel production, PhD dissertation, March 2011

83. Eric Ping, et al. [Paper in review].

84. Jones, A. and B. McNicol, Temperature-programmed reduction for solid materials characterization. 1986, New York: Marcel Dekker Inc.

85. Mile, B., et al., TPR studies of the effects of preparation conditions on supported nickel catalysts. Journal of Molecular Catalysis, 1990. 62(2): p. 179-198.

86. Mile, B., et al., The Location of Nickel-Oxide and Nickel in Silicasupported Catalysts – 2 Forms of NiO and the Assignment of Temperature-Programmed Reduction Profiles. Journal of Catalysis, 1988. 114(2): p. 217-229.

87. Marceau, E., et al., Nickel(II) Nitrate vs. Acetate: Influence of the Precursor on the Structure and Reducibility of Ni/MCM-41 and Ni/Al-MCM-41 Catalysts. Chemcatchem, 2010. 2(4): p. 413-422.

88. Godelitsas, A., et al., Characterisation of zeolitic materials with a HEU-type structure modified by transition metal elements: Definition of acid sites in nickelloaded crystals in the light of experimental and quantum-chemical results. Chemistry-a European Journal, 2001. 7(17): p. 3705-3721.

89. Chen, J.X., et al., An approach to preparing highly dispersed Ni2P/SiO2 catalyst. Catalysis Communications, 2010. 11(6): p. 571-575.

90. Tomiyama, S., et al., Preparation of Ni/SiO2 catalyst with high thermal stability for CO2-reforming of CH4. Applied Catalysis A: General, 2003. 241(1-2): p. 349-361.

91. Burattin, P., M. Che, and C. Louis, Characterization of the Ni(II) phase formed on silica upon deposition-precipitation. Journal of Physical Chemistry B, 1997. 101(36): p. 7060-7074.

92. Burattin, P., M. Che, and C. Louis, Molecular approach to the mechanism of deposition - Precipitation of the Ni(II) phase on silica. Journal of Physical Chemistry B, 1998. 102(15): p. 2722-2732.

93. M. A. Shah, A Versatile Route for the Synthesis of Nickel Oxide Nanostructures Without Organics at Low Temperature, Nanoscale Research Letters, 10.1007/s11671-008-9147-z

94. Yejun Qiu, Jie Yu, Xiaosong Zhou, Cuili Tan and Jing Yin, Synthesis of Porous NiO and ZnO Submicro- and Nanofibers from Electrospun Polymer Fiber Templates, Nanoscale Research Letters, 10.1007/s11671-008-9221-6

95. P. Burattin, M. Che and C. Louis, Charaterization of the Ni (II) Phase Formed on Silica Upon Deposition-Precipitation, J. Phys. Chem. B 1997, 101, 7060-7074

96. M. Tanaka, A. Itadani, Y. Kuroda and M. Iwamoto, Effect of Pore Size and Nickel Content of Ni-MCM-41 on Catalytic Activity for Ethene Dimerization and Local Structures of Nickel Ions, J. Phys. Chem. C 2012 10. 1021

97. Zhao, H. Y.; Li, D.; Bui, P.; Oyama, S. T. Hydrodeoxygenation of guaiacol as model compound for pyrolysis oil on transition metal phosphide hydroprocessing catalysts. Appl. Catal. A: Gen. 2011, 391 (12), 305−310.

98. A. L. Jongerius et al. CoMo sulfide-catalyzed hydrodeoxygenation of lignin model compounds: An extended reaction network for the conversion of monomeric and dimeric substrates, Journal of Catalysis 285 (2012) 315–323

99. ROBERT L. BURWELL, JR, THE CLEAVAGE OF ETHERS, Department of Chemistry, Northwestern University, Evanston, Illinois

100. A. G. Sergeev et al. A Heterogeneous Nickel Catalyst for the Hydrogenolysis of Aryl Ethers without Arene Hydrogenation, J. Am. Chem. Soc. 2012, 134, 20226−20229

101. Mesocellular-foam-silica-supported Ni catalyst: Effect of pore size on H_2 production from cellulose pyrolysis, International Journal of Hydrogen Energy Volume 37, Issue 12, June 2012, Pages 9590–9601

102. I. Kagehira, The Catalytic Hydrogenation of Aromatic Hydrocarbons under High Pressure and High Temperature, September, 1931

103. E. V. Uzee, H. Dkins, Hydrogenation and Hydrogenolysis of Ethers, Communication from the Laboratory of Organic Chemistry of the University of Wisconsin, Jan, 1935

104. K. C. Hou et al. The Kinetics of Thermal Decomposition of Benzene in a Flow System, The Joumal of f'hysical Chemietry, Volume 69, Sumber S March I966

105. ELMER B. LEDESMA et al. AN EXPERIMENTAL STUDY ON THE THERMAL DECOMPOSITION OF CATECHOL, Proceedings of the Combustion Institute, Volume 29, 2002/pp. 2299–2306

106. X. Wang, R. Rinaldi, Exploiting H-transfer reactions with RANEY Ni for upgrade of phenolic and aromatic biorefinery feeds under unusual, low-severity conditions, Energy Environ. Sci., 2012, 5, 8244-8260